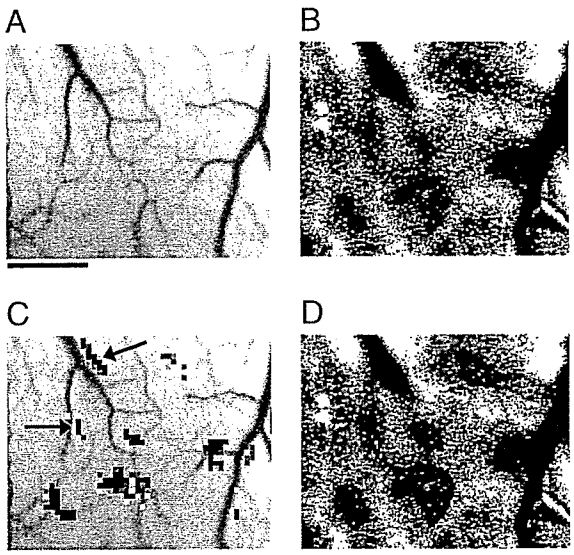

FIG. 1. Intrinsic signal imaging detected local modulation of light absorption changes in area TE. *A*: surface view of the exposed portion of the cortex. *B*: differential image showing local increase in light absorption. *C*: regions that showed statistically significant darkening after presentation of a visual stimulus are indicated in red ($P < 0.05$). Apparent artifacts that appeared along the thick vessels (arrows) were eliminated from the analysis. *D*: extracted active spots outlined by connecting pixels with half the peak absorption value. Scale bar = 1 mm.

mm and contained 320 × 240 pixels. We presented a visual stimulus to the monkey for 2.0 s, and sequential images were acquired for 4.0 s (starting from 1.0 s before the stimulus onset). During the 2-s stimulus presentation period, a stimulus image appeared and moved in a circular path (with a radius of 0.4° at the rate of 1 cycle/s). The imaging experiments consisted of two sessions. In the first session, the visual stimuli were 10–20 object images together with two blank images as control. Then on the basis on these results, we selected several stimuli that activated a large number of spots in the imaged region. In the second session, the selected stimuli ("the original"), their modifications and two controls were used as visual stimuli. Each stimulus was randomly presented 15–30 times in one session. The same imaging session as the second session was repeated at least twice on different days to confirm the consistency of the observed spots.

Identification of the active spots

The active spots were extracted as follows (Tsunoda et al. 2001): *1*) images acquired during the 0.5- to 3.0-s period after the onset of stimulus presentation were divided by an average of images during the 1-s period just before the stimulus onset. *2*) Gaussian spatial filtering was used to eliminate the global (stimulus nonspecific) darkening and high-frequency noise (cut-off frequencies: $\sigma = 0.04$ mm^{-1} for high cut and $\sigma = 2.1$ mm^{-1} for low cut). *3*) The *t*-values were calculated by pixel-by-pixel comparison of signal intensity between the filtered images for the trials with a particular stimulus and those for the control trials. The filtered images with a stimulus were averaged for all the trials and a differential image was created by subtracting the averaged image for control trials. Localized dark regions of the differential image, which showed significant darkening (*t*-test, $P < 0.05$), were defined as active spots. *4*) The contour of active spots was demarcated at the half-value of the peak absorption value. Representative images for each step are shown in Fig. 1.

Extracellular recording

The exposed cortex used for intrinsic signal imaging was covered with a transparent artificial dura made of silicon rubber (Arieli et al. 2002). Tungsten microelectrodes were inserted into the spots through the artificial dura. The surface blood vessel pattern was used as a mapping reference to identify the position of the spots. Extracellular action potentials were recorded for 3 s in each trial. Visual stimulus presentation started 1 s after the onset of a trial and lasted for 1 s. During the 1-s stimulus-presentation period, a stimulus image appeared and moved in a circular path (with a radius of 0.4° at the rate of 1 cycle/s). No intertrial interval was inserted, so that a blank period between two stimuli was 2 s. The different stimuli were presented in pseudo-random order, and the number of trials for each stimulus was between 10 and 20. For each stimulus, we applied the Wilcoxon test to the difference in the mean firing rate during and before the stimulus presentation. The amplitude of evoked responses for each stimulus was calculated by subtracting the mean firing rate during the 1-s period before the stimulus onset from the mean firing rate during the 1-s stimulus-presentation period, and by averaging for all the trials.

To characterize individual cells, we determined visual features critical for the cells according to previous studies (Fujita 1993; Fujita et al. 1992; Tanaka et al. 1991) (Fig. 2): *1*) we manually searched for the most effective visual stimulus among 96 hand-held 3D objects (Fig. 3), *2*) we simplified the best stimulus by removing or modifying a particular visual feature of the stimulus, and *3*) if the simplified image elicited significant responses (Wilcoxon test, $P < 0.05$) and also if the response amplitude for the simplified image exceeded a certain threshold, we used this image as the best stimulus in the next step. This procedure was repeated until further simplification failed to produce any response that exceeded the threshold. The threshold was set to 70% of the response elicited by the stimulus before simplification because there was no significant difference in evoked responses at this threshold. Typically, we started with the examination of a

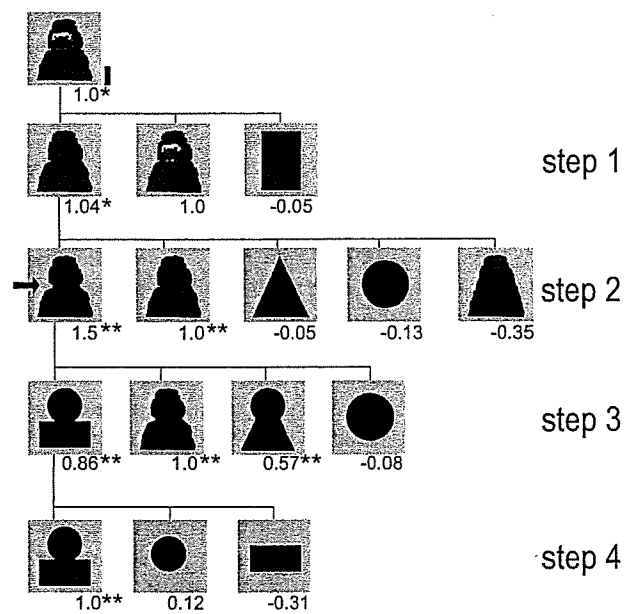

FIG. 2. Systematic simplification of an object image. The stimulus was simplified step by step. The stimulus that evoked the strongest response in one step was examined in the next step as the reference stimulus. The numbers below each picture indicate the response amplitudes normalized to the response to the reference stimulus together with statistical significance (Wilcoxon test, $*P < 0.05$, $**P < 0.01$). Step 1 showed that neuronal activities elicited by the best object and the silhouette were the same. Step 2 examined the effect of the 'sharpness' of the corner at the junction of upper and lower parts (arrow) and showed that the silhouette with the sharpest corners (leftmost picture) was the most effective stimulus. Step 3 showed that activities elicited by the leftmost two stimuli were not significantly different. Step 4 showed that neither the upper nor lower part activated the cell. In this case, the critical feature was determined as a combination of a circle and a rectangle (leftmost picture at step 4). Scale bar, 5°.

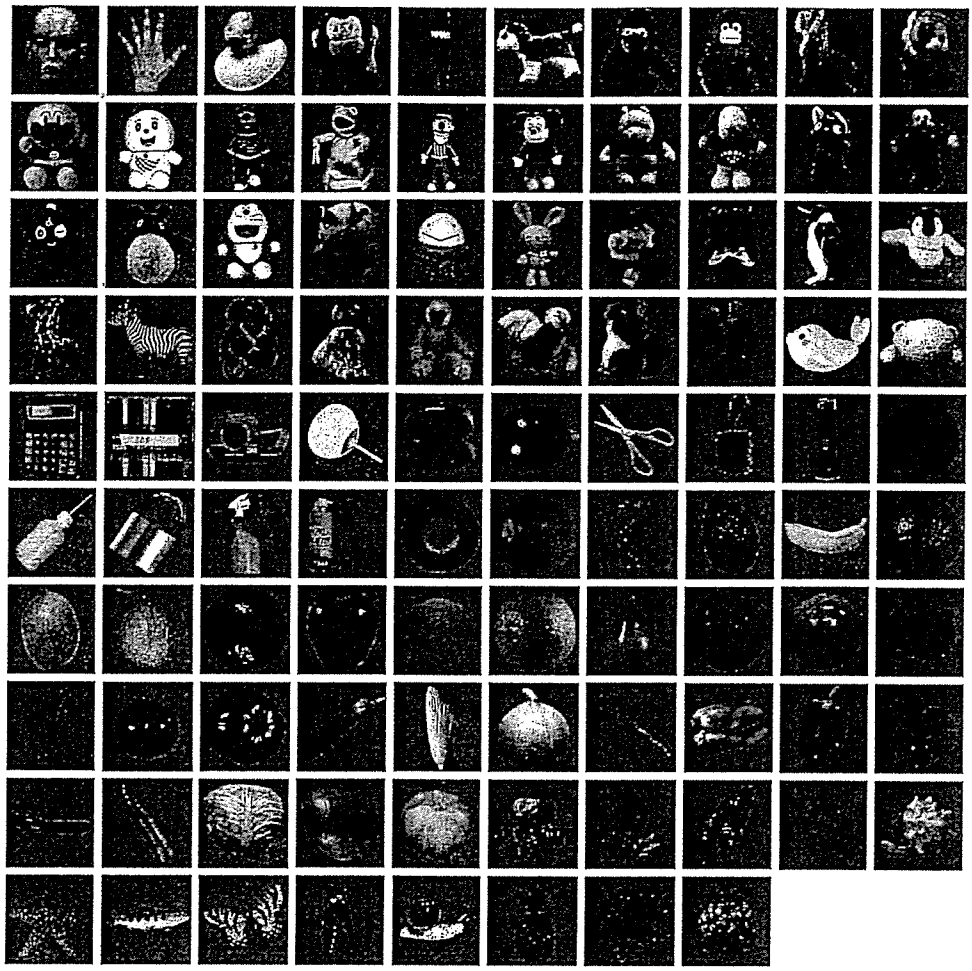

FIG. 3. The 3-dimensional (3D) objects used as visual stimuli to search for effective objects for individual cells. These objects were presented to the animals from various perspectives, as shown in the last three pineapple images in the *bottom row*.

monochrome image and silhouette of the original as in Fig. 2. However, image simplifications in the intermediate levels were different from case to case even if the original object was the same. The average numbers of simplification steps before reaching the simplest visual feature was 4.8 ± 2.0 (mean ± SD).

We examined receptive field size of each cell manually with the most effective 3D objects. We presented these objects not through the CRT display but directly to the animals because the size of receptive fields was larger than the size of the CRT display in most of the cells. On average, edges of receptive fields were 18.82 ± 8.17° above, 23.14 ± 5.30° below, 23.86 ± 8.41° contralateral, and 22.60 ± 8.62° ipsilateral to the recording hemisphere (means ± SD, $n = 35$). These values were measured from the center of the fovea. These values represent distances between the center of the CRT screen and the center of objects at the edges of receptive fields. Two exceptional cell having smaller receptive field size was eliminated from the analysis. The size of the object images used for quantitative analyses was on average 13.30 ± 3.08° along the vertical axis and was 10.88 ± 4.02° along the horizontal axis.

Definition of object parts

Throughout this manuscript, we took the simplest definition of object parts as the ones naturally distinguishable by discontinuities at minima of negative curvature of the object shape. For example, the minimum of negative curvature of stimulus 1 in Fig. 4*A* is the joint connecting head and body, and accordingly the stimulus is segmented into "head" (stimulus 3) and "body" (stimulus 2). Although this definition of parts is conventionally used in the field of object vision, there is no a priori reason to define object parts according to this definition for TE neurons. Our intention, however, was not to explore the optimal segmentation for TE neurons, but rather to search for a possible mechanism for representing the spatial relationship among local features.

RESULTS

Intrinsic signal imaging

First, using intrinsic signal imaging, we identified one or two visual stimuli that activated a large number of spots in an imaged region of area TE. Each of these "original" visual stimuli was segmented into parts containing local features. We then conducted another intrinsic signal imaging session with a stimulus set consisting of the original (stimulus 1), two individual parts of the original (stimuli 2 and 3), and the original with a gap between the two parts (stimulus 4; Fig. 4). The results revealed that each spot was activated differently by these four stimuli. For example, one spot (indicated by an arrowhead in Fig. 4*A*) was activated by stimuli 1, 3, and 4 but not by stimulus 2. We interpret activity in this spot as being related to local features in the upper part of the original image (Fig. 4*A*). Because we were interested in identifying spots related to the spatial arrangement of local features in parts, we restricted our analysis to spots that were activated by combinations of the two parts but not by individual parts. Among four examined hemispheres, we found three spots, A–C, that satisfied this criterion: these spots were activated by the original image (stimulus 1) and the original with a gap (stimulus 4)

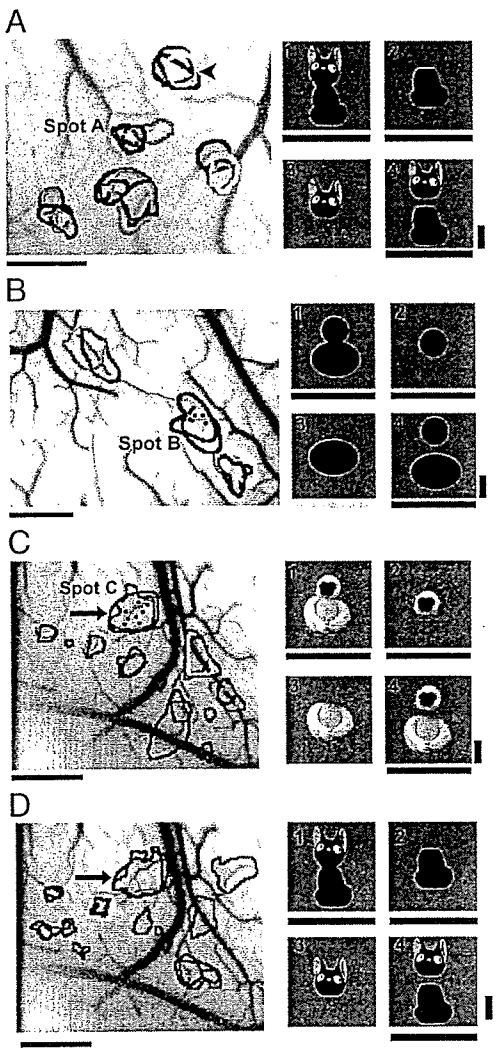

FIG. 4. Activation patterns of intrinsic signals evoked by sets of visual stimuli. *A–C*: activation patterns obtained from 3 different hemispheres, in which spots A, B, and C [spatial relationship relevant spots (SRR spots)] had specific response selectivity to sets of visual stimuli. *D*: activation pattern obtained from the same area of cortex shown in *C* but with a different set of stimuli. In each panel, activation patterns evoked by a set of the stimuli 1–4 (right) are indicated by colored contours superimposed on the surface image of the cortex. The bars below each stimulus and the outlines of spots activated by the stimulus match in color. The arrowhead in *A* indicates the spot related to local features in stimulus 3. The arrow in *D* indicates the region corresponding to spot C. The dots in the spots A–C indicate electrode penetration sites for subsequent extracellular recordings. Horizontal scale bar, 1 mm. Vertical scale bar, 5°.

but not by either part alone (stimuli 2 and 3; Fig. 4). Because the original with a gap (stimulus 4) activated these spots, activity in these spots could not be caused by specific responses to particular local features at the junction between the parts, such as a sharp negative curvature. We therefore considered these spots to be spatial relationship relevant spots (SRR spots), where we would likely find neurons representing the spatial relationship between two parts or between features within these parts.

Responses of the cells in SRR spots to spatial arrangements of object parts

We then conducted extracellular recordings from 49 cells located within SRR spots to characterize responsiveness of individual cells (13, 14, and 22 cells in spots A–C, respectively). First, we examined visual responses of each cell with 96 real object stimuli including faces, hands, imitations of living animals, stuffed animals, tools, and plastic fruits and vegetables (Fig. 3). These objects were presented in various sizes, orientations, and views so that the actual number of two-dimensional images used as visual stimuli was three or four times larger than the number of real objects. The stimuli that elicited significant responses (Wilcoxon test, $P < 0.05$) were diverse in color, texture, and local shapes (Fig. 5, *A, C,* and *E*). We could not explain this visual diversity in effective stimuli by preferred stimuli being different from cell to cell in a spot because individual cells in these spots responded to different stimuli and the response amplitudes did not significantly differ from each other (1-way ANOVA, $P > 0.25$; Fig. 5, *B, D,* and *F*). One common aspect of these effective visual stimuli was that the objects tend to consist of at least two distinguishable parts (Fig. 5, *B, D,* and *F*). These results from extracellular recordings were in accordance with the observation that with optical imaging, stimulus selectivity of a spot was the same for stimulus sets that originated from different object images (Fig. 4, *C* and *D*).

To address the question of whether cells in these spots could represent spatial relationships between object parts, we generated a set of visual stimuli for each cell where the upper part of the best object stimulus was rotated by various angles relative to the lower part of it. We then examined selectivity of each cell to this set of visual stimuli (Fig. 6). We found that cells were selectively activated when the parts were aligned vertically (Fig. 6, *A* and *B*). The selectivity could not be simply explained by changes in retinotopic positions of the upper parts that occurred incidentally during the spatial rearrangements of parts because of the large receptive field sizes of cells in area TE (Gross et al. 1969; Ito et al. 1995). In fact, evoked responses to the best object stimulus at different positions in space did not significantly differ from each other (Fig. 6*A*, symbols on the vertical axis). Of 30 cells examined for spatial arrangements of object parts, the responses of 20 cells (67%) significantly depended on the spatial configurations of two parts (1-way ANOVA, $P < 0.05$; Fig. 6, *C–F*). Thirteen cells had a single peak at 0 or 45° (Fig. 6, *C* and *D*), 4 cells had a single peak at other positions (Fig. 6*E*), and the remaining 3 cells had two peaks (Fig. 6*F*). Receptive field sizes of these cells were larger than the range of the shift of upper parts in retinotopic position incidental to the spatial rearrangement of parts (see METHODS). These results suggest that the cells in SRR spots are sensitive to particular spatial arrangements of objects' parts.

Response properties of the cells in SRR spots for the simplest visual features that activated the cells

The sensitivity of the cells to a particular spatial arrangement of parts could be due to the changes in local shapes of either part that occurred incidentally during spatial rearrangements of parts (for example, see Fig. 6, *A* and *B*). We conjectured that this was not the case because SRR spots were less sensitive to variations in local shapes (Fig. 5). To confirm this point, however, we determined the simplest visual feature that produced maximal activation ("critical feature"), and examined the cell's sensitivity to modifications of the critical feature for

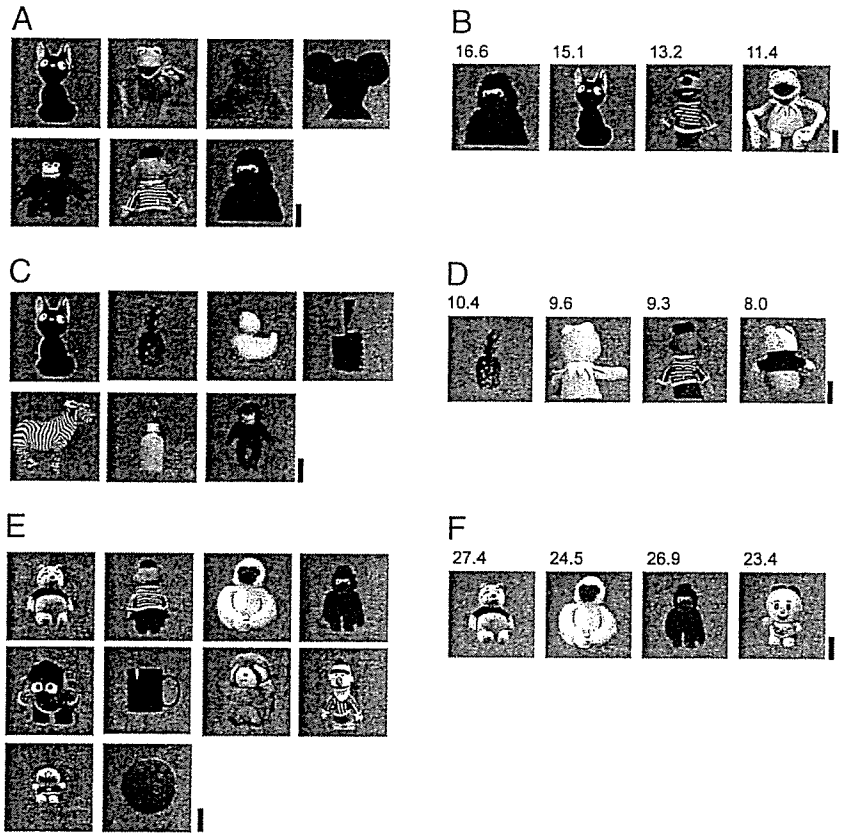

FIG. 5. Representative object stimuli that elicited significant responses of cells in SRR spots. *A*, *C*, and *E*: each object image represents the stimulus in a specific orientation that elicited the strongest significant responses out of the 96 objects in various orientations and views tested (*t*-test, $P < 0.05$) for a cell recorded in spots A (*A*), B (*C*), and C (*E*). *B*, *D*, and *F*: best 4 stimuli of 96 objects that elicited significant responses for a representative cell in spots A (*B*), B (*D*), and C (*F*). One-way ANOVA confirms no significant difference in responses to these 4 stimuli in both cases ($P > 0.25$). Evoked responses (spikes/s) are indicated above each stimulus image. Scale bar, 5°.

each cell in spots A and B. We systematically simplified the best object stimulus step by step to find critical features for 27 cells, following procedures from previous studies (Fujita 1993; Fujita et al. 1992; Kobatake and Tanaka 1994; Tanaka et al. 1991) (Fig. 2). Figure 7*A* shows the responses of a representative cell in spot A to its critical feature and to modifications of the critical feature. The critical feature was a combination of a circle and a rectangle (Fig. 7*A*, stimulus 1); the presentation of the upper or lower part alone caused significant decrease in the evoked responses (*t*-test, $P < 0.05$; Fig. 7*A*, stimuli 2 and 3). The cell responded equally well to the original colored object image and a silhouette of the original, indicating that color and texture of the stimulus were not essential (for example, see Fig. 2). The cell was not sensitive to changes in the shape of individual parts as long as the combination was preserved (Fig. 7*A*, stimuli 4 and 5). The existence of two parts was required, but the cell was not sensitive to local features at the junction between the two parts. For example, evoked responses to the stimulus with a gap (stimulus 7) and to the original (stimulus 1) were not significantly different (Fig. 7*A*). If, however, the "two parts" distinction was made less evident by smoothing the sharp joints (Fig. 7*A*, stimulus 8), the response was significantly reduced. Thus stimulus 6 but not stimulus 5 caused significant decrease in the evoked responses (Fig. 7*A*). The representative cell in spot B shows results consistent with the cell in spot A (Fig. 7*C*). In addition, we found that sharp joints between the two parts presented in isolation (Fig. 7*C*, stimulus 10) significantly reduced the responses, indicating that a sharp joint by itself was not sufficient.

Of 27 examined cells, the stimulus simplification revealed that 25 cells (93%) were not selective for color, luminance, or texture (exceptions are given in Fig. 7*B*, stimuli 5 and 6), and the critical features of 22 cells (81%) consisted of two parts (Fig. 7, *B* and *D*; exceptions are stimulus 8 in Fig. 7*B*, and stimuli 7 and 8 in Fig. 7*D*). The sensitivity of these neurons to modifications of critical features are summarized in the scatter plots, where diagonal lines indicate that evoked responses to the critical features and those to the modifications were the same (Fig. 8). Evoked responses to isolated parts were typically smaller than those to the critical features except for in a few cells (Fig. 8, *A* and *B*). The cells did not respond differently after changes in shape of either part or by inserting a gap between the two parts (Fig. 8, *C* and *D*). In 37% of the cells (filled symbols; 6 of 16 cells), significant reduction was observed when the stimuli had smoothed edges between the parts, but there was no significant reduction for the rest of the cells (open symbols; 10 of 16 cells) probably because two parts of the critical features were still distinguishable even when the joint was smoothed (Fig. 8*E*). Elongated shapes and a sharp joint between the two parts presented in isolation caused significant reductions in responses (Fig. 8, *F* and *G*). Thus sensitivity to these modifications of the critical features obtained from a population of neurons in these spots generally agreed with that obtained from representative cells.

In addition to the preceding results, as expected from the sensitivity of these cells to spatial arrangement of the object parts (Fig. 6), we found these cells were also sensitive to modifications of critical features in spatial arrangement of parts (Fig. 9). It should be noted that among the cells that were selective to a particular spatial arrangement of parts, 73% did

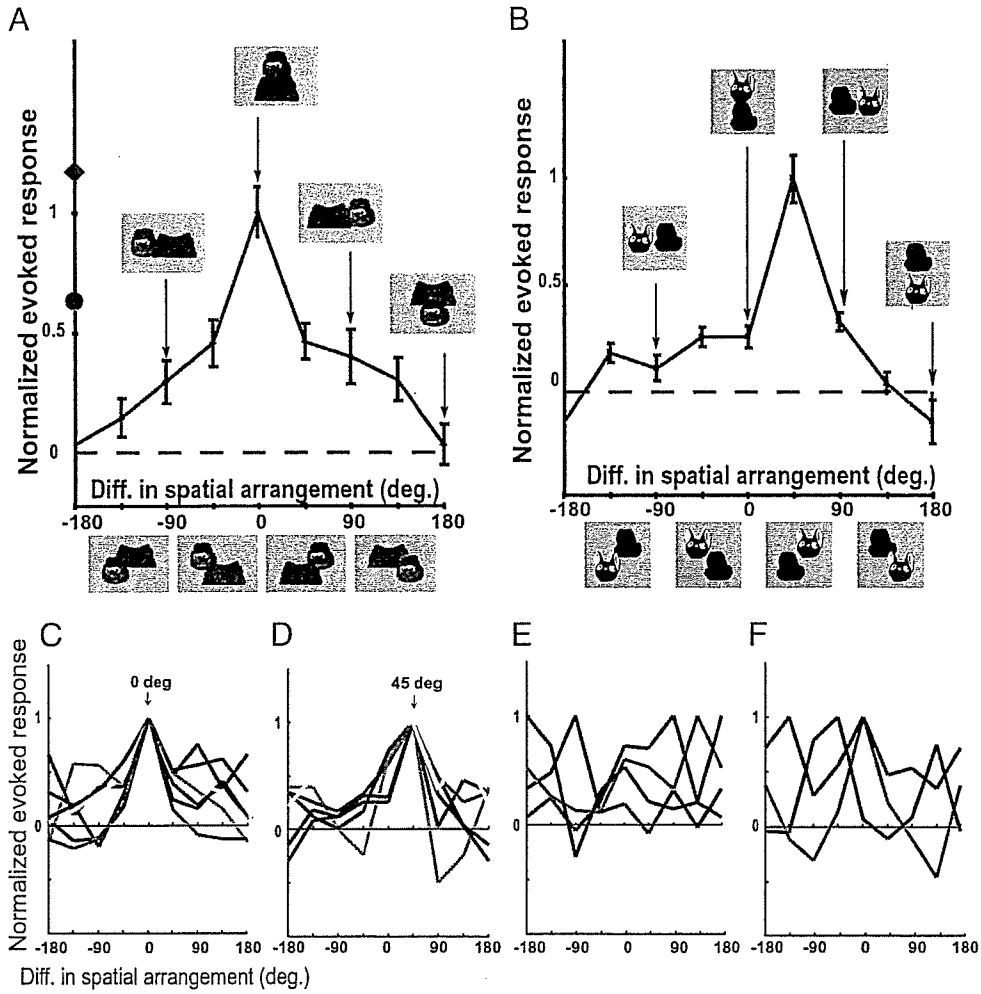

FIG. 6. Selectivity of cells in SRR spots to different spatial arrangements of the upper and the lower parts of object images. The normalized evoked responses (vertical axis) were plotted against the difference in the spatial arrangement of the parts (horizontal axis). The difference in spatial arrangement is defined by the angle between a line connecting the centers of the 2 parts of the best object stimuli and that of each rearranged stimulus. The pictures of stimuli corresponding to each angle are shown below the plot and also in the insets. *A* and *B*: responses of representative cells in spots A and B, respectively. Error bars indicate SE (n = 20). One-way ANOVA confirmed that the evoked responses significantly differed depending on the spatial arrangement of the parts ($P < 0.05$). Normalized responses to the original stimuli presented at different retinotopic positions are indicated by symbols along the vertical axis in *A*. The distance between the leftmost (●) and rightmost (◆) stimuli was 12.8°. *C–F*: tuning curves for other cells in spots A–C with a single peak at 0° (*C*), 45° (*D*), and other angles (*E*), and tuning curves with multiple peaks (*F*). For simplicity, only the mean values of responses are plotted.

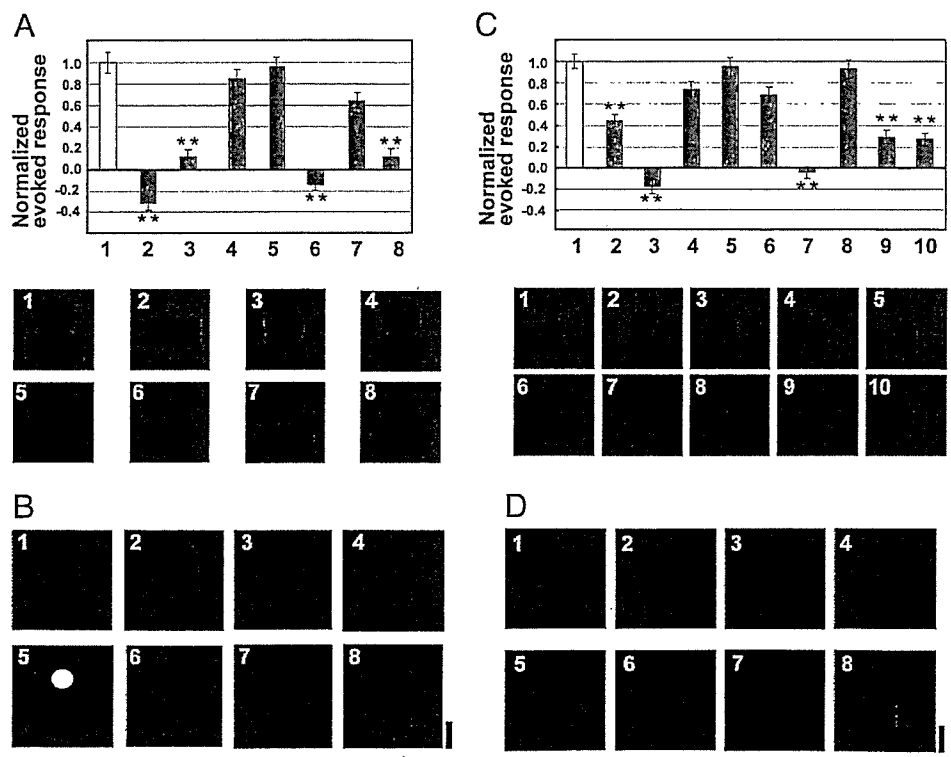

FIG. 7. Visual features critical for the cells in SRR spots. *A* and *C*: single-cell responses in spots A (*A*) and B (*C*). Evoked responses normalized to those by the critical features (stimulus 1) were plotted against the stimulus numbers. The pictures of stimuli with the stimulus number are shown below. Asterisks indicate a significant decrease in evoked responses compared with responses to the critical features (stimulus 1) (*t*-test, $P < 0.01$). Error bars indicate SE (n = 20). *B* and *D*: representative critical features for different cells in spots A (*B*) and B (*D*). The stimulus was filled with black if color, luminance, and texture were not essential for activation. Only the cells with critical features 5 and 6 (*B*) were sensitive to luminance. Scale bar, 5°.

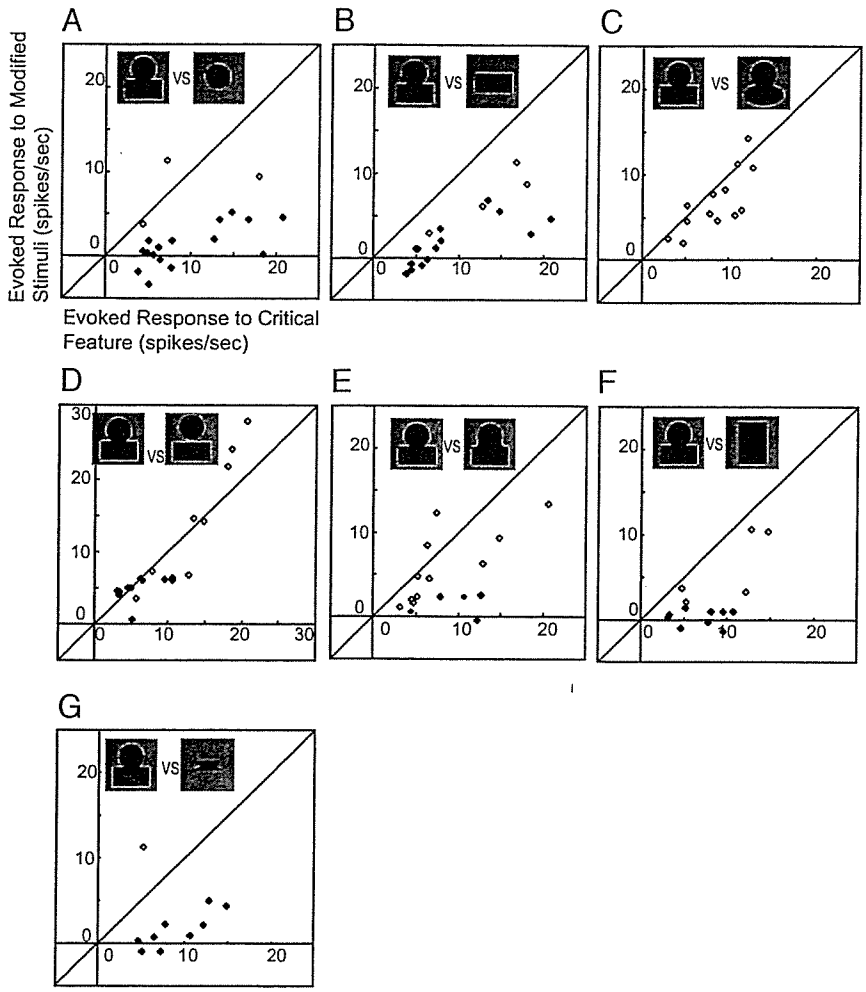

FIG. 8. Comparison between responses to the critical features and those to the modifications of the critical features. The modifications were isolated parts (A, *top*, and *B, bottom*), changes in shape of parts (*C*), inserting a gap between parts (*D*), smoothing the sharp joint (*E*), elongated shape (*F*), and isolated sharp joint (*G*). These modifications are signified by icons at the top of each graph, but these icons were not exactly the ones used in the experiment. The actual stimuli were created by modifying the critical features of individual cells. Each point represents the evoked response of single cell to its critical feature (horizontal axis) and that to modifications (vertical axis). Points below (or above) the diagonal line indicate that the response to the modification was smaller (or larger) than the response to the original critical feature. Filled symbols represent the cells that showed a significant difference in response to critical features and the modifications. These single cellular responses were obtained from spots A (red symbols) and B (blue symbols).

not respond to the combination of parts when the upper part was rotated 180° (Figs. 6 and 9). This means that, although neurons in these spots are less sensitive to local features, they still possess the capability to distinguish upper parts from lower parts by certain features existing within the parts. Because the upper and lower parts of each critical feature were different in size for most of these cells (Fig. 7, *B* and *D*), relative size may be one determining factor.

Taken together, at the level of the simplest visual features that maximally activate individual cells, we found that cells in SRR spots required two distinguishable parts for activation. For maximal activation of these cells, these two parts had to be arranged in particular spatial configurations, but it was not necessary to have particular local features embedded in parts.

DISCUSSION

It has been shown that object images are represented by combinations of neurons representing component visual features that are less complex than object images in IT cortex (Desimone et al. 1984; Fujita 1993; Fujita et al. 1992; Ito et al. 1995; Kobatake and Tanaka 1994; Tanaka et al. 1991; Tsunoda et al. 2001; Wang et al. 1996, 1998). As for the spot indicated by the arrowhead in Fig. 4*A*, some of these neurons represent local features of object images (see also Tsunoda et al. 2001). Thus for complete reconstruction of an object image from these features, neural mechanisms that specify spatial configuration of these local features are needed. A general framework of object representation is the structural description where object images are composed of parts and the spatial relation among parts (Biederman 1987; Marr and Nishihara 1978). Although parts in this general framework and visual features represented in IT cortex are not necessarily the same, the representation of spatial configuration of elementary components is the common central issue.

Recently, Brincat and Connor examined visual responses of IT neurons with variations of two-dimensional (2D) silhouettes consisting of multiple curvatures and found that optimal features of these neurons were a combination of specific local curvatures arranged in particular positions in space (Brincat and Connor 2004). In this study, they examined the cells with 2D silhouettes but not with object images. Because representation of spatial configuration requires the cell to be insensitive to the visual attributes specific to particular parts, their results were not conclusive with respect to representation of spatial configuration of object parts.

From our findings in the present study, we suggest that neurons in area TE could represent a particular spatial arrangement of object parts based on two observations: *1*) with intrinsic signal imaging, we found activity spots that responded to a combination of two parts but not to either part shown in isolation (Fig. 4) and *2*) neurons recorded in these SRR spots were selectively activated by stimuli in which the parts were

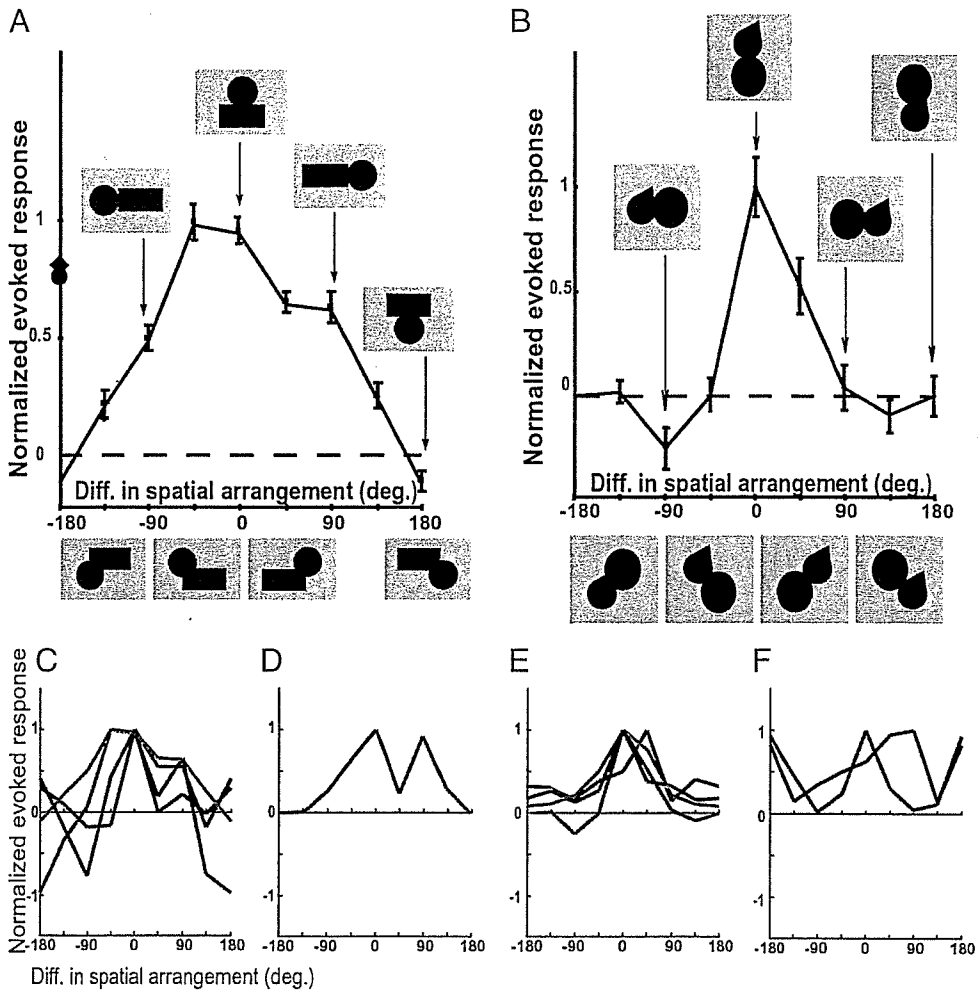

FIG. 9. Selectivity of cells in SRR spots to different spatial arrangements of the upper and the lower parts of their critical features. Normalized responses of the representative cells in Fig. 6, *A* and *B*, are represented in *A* and *B*, respectively. The stimuli were generated from the critical feature of each cell instead of the best object stimulus. Other conventions are the same as those in Fig. 6. One-way ANOVA confirmed that the evoked responses significantly differed depending on the spatial arrangement of the parts ($P < 0.05$). Normalized responses to the critical feature presented at different retinotopic positions are indicated by symbols along the vertical axis in *A*. The distance between the leftmost (●) and rightmost (◆) stimuli was 12.8° (*C–F*). Tuning curves for other cells with single (*C* and *E*) and multiple peaks (*D* and *F*) in spots A (*C* and *D*) and B (*E* and *F*).

arranged in specific spatial relationship (Figs. 6 and 9). In addition, our data show that cells in these spots are less sensitive to changes in visual attributes that are essential to characterize local features, such as color, texture, and local shape: *1*) activity spots showed the same response selectivity for stimulus sets derived from different object images (Fig. 4, *C* and *D*), *2*) neurons in these spots responded equally well to the stimuli including different colors, textures, and local shapes (Fig. 5), and *3*) the critical features of these neurons did not include particular local features (Fig. 7, *B* and *D;* see also Fig. 2). These two sets of results suggest that neurons in these spots were activated when arbitrary local features were arranged in a particular spatial configuration. Further evidence supporting this view is provided by direct comparison between responses to variations in color, texture, and local shape of parts and those to variations in the spatial arrangements of parts: the cells in SRR spots were more selective to particular spatial arrangements of parts than to examined variations in color, texture, and shape (Fig. 10). Therefore in terms of representation of object images, the neurons characterized in this study could play a role in specifying spatial relationships between parts. Altogether we found only four SRR spots among 26 activity spots elicited by "original" object images (16.7%). This relatively small proportion indicates that an object image consists of multiple local features and different types of spatial configurations. In the present study, we only investigated neural representation of one particular type of spatial configuration: two parts aligned vertically. It should be noted that these spots did not respond to the combination of parts when the upper part was rotated 180° (Figs. 6, *C* and *D*, and 9, *C* and *E*), indicating that these neurons are capable of differentiating two parts. Sensitivity of the cells to some unidentified local cues could be essential for differentiating two parts. Further investigations will be necessary to fully understand the neural representation of spatial relationships among parts or local features in general.

Multiple studies with anesthetized as well as alert monkeys have shown that on average, cells in area TE have large receptive fields (Ito et al. 1995; Kobatake and Tanaka 1994; Op De Beeck and Vogels 2000). However, some reports shows that the size of receptive fields of IT cells could be a small portion of the visual field (DiCarlo and Maunsell 2002; also see Op De Beeck and Vogels 2000). Thus one may consider that the sensitivity to a particular spatial arrangement of parts (Figs. 6, 9, and 10) is simply due to upper parts of stimuli falling out of the receptive fields when upper parts were rotated relative to lower parts. One determining factor of receptive field size is the size of stimuli used in these investigations; it has been reported that the size of receptive fields increases when the size of stimuli increases (Ito et al. 1995; Op De Beeck and Vogels 2000). DiCarlo and Maunsell (2002) used stimuli as small as 0.6° but Kobatake and Tanaka (1994) used the stimuli as large as 10°. In the present study, we hand-plotted a receptive field for each cell; on average, receptive fields were as large as 42 × 46°. The stimulus size in our study was 13.3 × 10.9° on

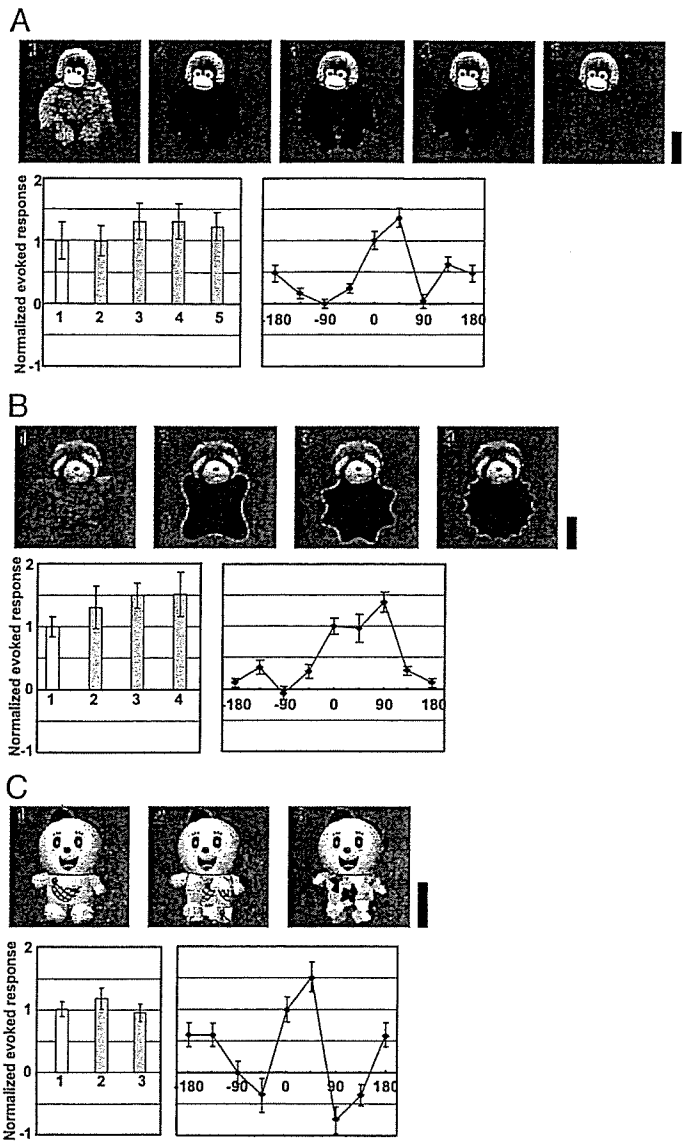

FIG. 10. Tuning specificity of representative neurons to stimuli in which lower parts were filled with different colors (*A*), had different shapes (*B*) or had altered textures (*C*). *A*: tuning specificity for color was examined for red (17.6, 0.506, 0.366), blue (11.7, 0.187, 0.213), green (19.3, 0.278, 0.518), and yellow (32.5, 0.399, 0.491). *Top*: [the numbers in the parentheses give the values for luminance (*Y*), and chromaticity coordinate (*x*, *y*) in CIE color space]. Among 10 cells (6 and 4 cells tested on changes to the *bottom* and *top*, respectively), no cell showed evoked responses that significantly depended on different colors, except for 3 cells tested on changes to the *top* (1-way ANOVA, $P > 0.1$). *B*: tuning specificity for shape was examined with Fourier descriptor stimuli (frequency, 4, 8, and 16; amplitude, 0.8) (*top*). Among 5 cells (4 and 1 cells tested on changes to the *bottom* and *top*, respectively), no cell showed evoked responses that significantly depended on shape (1-way ANOVA, $P > 0.1$). *C*: tuning specificity for texture was examined using stimuli in which the texture within one of the parts was modified. To create coarse texture modification, we partitioned either part of the stimulus into nine rectangular regions and shuffled them (stimulus 2). To create fine texture modification, we first made a Voronoi diagram based on randomly chosen pixels that were at most separated by 1.1° of visual angle. Then each area of the Voronoi region was filled with the color of the pixel which was its own base point (stimulus 3). Among 8 cells (5 and 3 cells tested on modifications to the *bottom* and *top*, respectively), only 2 cells showed evoked responses that significantly depended on differences in texture in either part (1-way ANOVA, $P > 0.1$). *A*—*C*, recorded from different neurons. In all figures, upper panel shows the stimuli, the *bottom left panel* shows evoked responses to these stimuli normalized to the responses elicited by the original best object image and *bottom right*: the tuning specificity of the same neuron to different spatial arrangements of parts of the best object for that cell. All of these cells were sensitive to particular spatial arrangements of parts. Scale bar, 5°.

average. Thus it is less possible that our results (Figs. 6, 9, and 10) are due to a decrease of responses when the stimuli fell out of the small receptive field, although quantitative analysis of the receptive field for neurons in SRR spots would be necessary in the future.

Finally, although it has been reported that many neurons in area TE respond to visual features less complex than natural objects, it has remained unclear whether these features are related to local features of object images or to more global features (Fujita 1993; Fujita et al. 1992; Ito et al. 1995; Kobatake and Tanaka 1994; Tanaka et al. 1991). Here, by global features we mean the combination of elementary components such as combinations of color and shape and local features. In particular, specification of spatial relationship among parts is one such global features. One important contribution of the present study is that it provides concrete evidence that critical features can be such global features of object images.

ACKNOWLEDGMENTS

We thank Dr. Etsuro Ito for providing an opportunity for Y. Yamane to conduct this study and for continuous encouragement throughout the study. The authors thank Drs. Kathleen Rockland, Uma R. Maheswari, and Bonnie Lee La Madeleine for helpful comments on an earlier version of the manuscript. We also thank Dr. Ryota Homma for technical support and suggestions.

GRANTS

This work was partly supported by Research Fellowships of the Japan Society for the Promotion of Young Scientists to Y. Yamane.

REFERENCES

Arieli A, Grinvald A, and Slovin H. Dural substitute for long-term imaging of cortical activity in behaving monkeys and its clinical implications. *J Neurosci Methods* 114: 119–133, 2002.

Biederman I. Recognition-by-components: a theory of human image understanding. *Psychol Rev* 94: 115–147, 1987.

Brincat SL and Connor CE. Underlying principles of visual shape selectivity in posterior inferotemporal cortex. *Nat Neurosci* 7: 880–886, 2004.

Bruce C, Desimone R, and Gross CG. Visual properties of neurons in a polysensory area in superior temporal sulcus of the macaque. *J Neurophysiol* 46: 369–384, 1981.

Desimone R, Albright TD, Gross CG, and Bruce C. Stimulus-selective properties of inferior temporal neurons in the macaque. *J Neurosci* 4: 2051–2062, 1984.

DiCarlo JJ and Maunsell JHR. Anterior inferotemporal neurons of monkeys engaged in object recognition can be highly sensitive to object retinal position. *J Neurophysiol* 89: 3264–3278, 2002.

Fujita I. Columns in the inferotemporal cortex: machinery for visual representation of objects. *Biomed Res* 14: 21, 1993.

Fujita I, Tanaka K, Ito M, and Cheng K. Columns for visual features of objects in monkey inferotemporal cortex. *Nature* 360: 343–346, 1992.

Gochin PM, Miller EK, Gross CG, and Gerstein GL. Functional interactions among neurons in inferior temporal cortex of the awake macaque. *Exp Brain Res* 84: 505–516, 1991.

Gross CG. How inferior temporal cortex became a visual area. *Cereb Cortex* 5: 455–469, 1994.

Gross CG, Bender DB, and Rocha-Miranda CE. Visual receptive fields of neurons in inferotemporal cortex of the monkey. *Science* 166: 1303–1306, 1969.

Gross CG, Bender DB, and Gerstein GL. Activity of inferior temporal neurons in behaving monkeys. *Neuropsychology* 17: 215–229, 1979.

Ito M, Tamura H, Fujita I, and Tanaka K. Size and position invariance of neuronal responses in monkey inferotemporal cortex. *J Neurophysiol* 73: 218–226, 1995.

Kobatake E and Tanaka K. Neuronal selectivities to complex object features in the ventral visual pathway of the macaque cerebral cortex. *J Neurophysiol* 71: 856–867, 1994.

Logothetis NK and Sheinberg DL. Visual object recognition. *Annu Rev Neurosci* 19: 577–621, 1996.

Marr D and Nishihara HK. Representation and recognition of the spatial organization of three-dimensional shapes. *Proc R Soc Lond B Biol Sci* 200: 269–294, 1978.

Op De Beeck H and Vogels R. Spatial sensitivity of macaque inferior temporal neurons. *J Comp Neurol* 426: 505–518, 2000.

Perrett DI, Rolls ET, and Caan W. Visual neurones responsive to faces in the monkey temporal cortex. *Exp Brain Res* 47: 329–342, 1982.

Schwartz EL, Desimone R, Albright TD, and Gross CG. Shape recognition and inferior temporal neurons. *Proc Natl Acad Sci USA* 80: 5776–5778, 1983.

Tanaka K, Saito H, Fukada Y, and Moriya M. Coding visual images of objects in the inferotemporal cortex of the macaque monkey. *J Neurophysiol* 66: 170–189, 1991.

Tsunoda K, Yamane Y, Nishizaki M, and Tanifuji M. Complex objects are represented in macaque inferotemporal cortex by the combination of feature columns. *Nat Neurosci* 4: 832–838, 2001.

Wang G, Tanaka K, and Tanifuji M. Optical imaging of functional organization in the monkey inferotemporal cortex. *Science* 272: 1665–1668, 1996.

Wang G, Tanifuji M, and Tanaka K. Functional architecture in monkey inferotemporal cortex revealed by in vivo optical imaging. *Neurosci Res* 32: 33–46, 1998.

Zahn CT and Roskies RZL. Fourier descriptors for plane closed curves. *IEEE Trans Comput* 21: 269–281, 1972.

1apraid4/z7g-iovs/z7g-iovs/z7g00507/z7g8167d07a | moyerr | S=11 | 3/6/07 | 19:07 | Art: 06-1294 | Input-mr

Intrinsic Signal Imaging in Macaque Retina Reveals Different Types of Flash-Induced Light Reflectance Changes of Different Origins

AQ: 1

Gen Hanazono,[1,2] Kazushige Tsunoda,[1,2] Kei Shinoda,[1] Kazuo Tsubota,[3] Yozo Miyake,[1] and Manabu Tanifuji[2]

Purpose. Intrinsic signal imaging is a newly developed technique that can map the light reflectance changes of tissues noninvasively. It has been used to map the functional organization of the retina by recording light-induced changes in the cone and rod photoreceptors. The purpose of this study was to investigate the properties of the intrinsic signals in the monkey's retina. To accomplish this, the intrinsic signals and the electroretinograms (ERGs) evoked by the same stimuli were measured under different recording conditions.

AQ: 2

Methods. The fundus of macaque monkeys was observed with infrared light and recorded with a charge-coupled device (CCD) camera. The intrinsic signals were measured as retinal light reflectance changes induced by diffuse or focal flash stimuli. ERGs were recorded under the same stimulating conditions. The reflectance changes induced by different flash intensities, flash intervals, and background luminance were compared.

Results. The intrinsic signals were categorized into different groups based on the location in the fundus. Fast signals (peak: ~100 ms) were recorded from the posterior retina including the fovea, and slow signals (peak: 5.0–6.0 seconds) were recorded from the optic disc and nonfoveal posterior retina. The threshold of the slow signal changes was comparable to that of the ERG b-wave, and the thresholds of the fast signals were higher than that of the ERG a- and b-waves.

Conclusions. The retinal intrinsic signals are composed of several components with different response properties and different sources. This recording technique may be useful for mapping the retinal function in eyes with various disorders. (*Invest Ophthalmol Vis Sci.* 2007;48:000–000) DOI:10.1167/iovs.06-1294

Assessing the functional properties of the retina objectively is essential for making a correct diagnosis and prognosis in various retinal disorders. Although recent advances in imaging techniques—for example, optical coherence tomography (OCT),[1,2] have revealed the morphologic changes in retinal structures, the functional properties of the retina cannot be evaluated with these imaging techniques. Thus, the electroretinogram (ERG) is still the only practical method of assessing neural activities in the retina.

Intrinsic signal imaging is a well-established imaging technique that translates neural activity into a visual image. This method measures the stimulus-induced light reflectance changes in tissues and has recently been used to assess the cone- and rod-induced retinal responsiveness in macaque monkeys.[3] It has also been used to examine the near-infrared reflectance changes in the human retina[4–6] and optic nerve head.[7] This noninvasive objective technique has good potential for development as a tool for the early detection of retinal dysfunction in cases of age-related macular degeneration, retinitis pigmentosa, and other retinal diseases.

However, before this tool can be brought into the clinic, a detailed knowledge of the properties and origin of the signals obtained by intrinsic signal imaging is necessary. Based on past investigations of intrinsic signal imaging in the cerebral cortex, the decrease in light reflectance (i.e., darkening after a visual stimulus) correlates strongly with local neural activity.[8–11] In the retina, however, the source and the properties of the intrinsic signals appeared to be more complex than in the cerebral cortex due to its complex layered structure.[3]

The purpose of this study was to investigate the basic properties of the retinal intrinsic signals. To accomplish this, we recorded the intrinsic signals of the macaque retina and ERGs under various recording conditions but using the same diffuse flash stimulus. In addition, we recorded the intrinsic signals evoked by focal flash stimuli. The results indicate that the intrinsic signal of the monkey's retina is composed of different components that originate in different layers of the retina.

Methods

The procedures used to record the intrinsic signals have been described in detail.[3]

The experiments were performed on two Rhesus monkeys (*Macaca mulatta*) and one Japanese monkey (*Macaca fuscata*). The results from monkeys 1 and 2 are shown in Figures 1 trough 5, and those from monkey 3 in Figures 6 and 7. After an intramuscular injection of atropine sulfate (0.08 mg/kg), the monkeys were anesthetized with droperidol (0.25 mg/kg) and ketamine (5.0 mg/kg) and then paralyzed with vecuronium bromide (0.1–0.2 mg/kg per hour). They were artificially ventilated with a mixture of 70% N_2O, 30% O_2, and 1.0% to 1.5% of isoflurane. The EEGs, ECGs, expired CO_2, and rectal temperature were monitored continuously throughout the experiments. Before the recordings, the pupils were fully dilated with topical tropicamide (0.5%) and phenylephrine hydrochloride (0.5%). The experimental protocol was approved by the Experimental Animal Committee of the Riken Institute, and all experimental procedures were performed in accordance with the guidelines of the Riken Institute and the ARVO Statement for the Use of Animals in Ophthalmic and Vision Research.

From the [1]Laboratory of Visual Physiology, National Institute of Sensory Organs, Tokyo, Japan; the [2]Laboratory for Integrative Neural Systems, Brain Science Institute, RIKEN, Saitama, Japan; and the [3]Department of Ophthalmology, Keio University School of Medicine, Tokyo, Japan.

Supported by Researches on Sensory and Communicative Disorders from the Ministry of Health, Labor, and Welfare, Japan.

Submitted for publication October 27, 2006; revised December 28, 2006; accepted Month, Day, 2007.

Disclosure: **G. Hanazono**, None; **K. Tsunoda**, None; **K. Shinoda**, None; **K. Tsubota**, None; **Y. Miyake**, None; **M. Tanifuji**, None

The publication costs of this article were defrayed in part by page charge payment. This article must therefore be marked "*advertisement*" in accordance with 18 U.S.C. §1734 solely to indicate this fact.

Corresponding author: Kazushige Tsunoda, Laboratory of Visual Physiology, National Institute of Sensory Organs, Tokyo Japan, 2-5-1 Higashigaoka, Meguroku, Tokyo 1528902, Japan; tsunodakazushige@kankakuki.go.jp.

ARTICLE TYPE: VNEU

tapraid4/z7g-iovs/z7g-iovs/z7g00507/z7g8167d07a | moyerr | S=11 | 3/6/07 | 19:07 | Art: 06-1294 | Input-mr

Intrinsic Signal Imaging and Data Analyses

A modified digital fundus camera system (NM-1000; Nidek, Aichi, Japan) was used to observe and measure the light reflectance changes from the ocular fundus. The fundus images were recorded with a charge-coupled device (CCD) camera (PX-30BC; Primetech Engineering, Tokyo, Japan), and the images were digitized with an IBM-compatible computer equipped with a video framegrabber board (gray-level resolution, 10 bits; spatial resolution, 640 × 480; temporal resolution, one-thirtieth of a second; Corona II; Matrox, Quebec, Canada). The camera was focused on the macular vessels, and the area recorded covered 45°, which included the macula; the superior and inferior vascular arcades, and the optic disc. We mainly investigated three retinal sites: the fovea, the posterior retina between the macula and inferior temporal artery, and the optic disc (Fig. 1A).

The fundus was continuously monitored with light from a halogen lamp filtered through an infrared interference filter (840–900 nm). Visible light could not be used for fundus monitoring because the light reflectance changes induced by bleaching of the photopigments have a polarity opposite to that of the intrinsic signals,[5,12–16] leading to incorrect mapping of the stimulus-evoked responses topographically.

Each recording trial consisted of 300 video frames collected at 30 frames per second for a total recording time of 10 seconds. To determine the time course of the flash-induced reflectance changes, we averaged the gray-scale values of 15 video frames collected in 0.5 second for each of the data points (Figs. 1, 6, and 7).

An unfiltered Xenon flash (duration: 1 ms) was given to the whole posterior pole of the ocular fundus or to a focal region of the posterior retina, 500 ms after the initiation of data acquisition. The maximum flash intensity (0-log-unit intensity) measured at the cornea was 308.0 cd · s/m^2 (measured at 50.2 mm from the object lens, by a photoradiometer; model IL-1700; International Light Technologies Inc., Peabody, MA). The timing of the data acquisition and stimulus delivery was under computer control.

Changes in light reflectance from the ocular fundus after the stimulus, such as a darkening (a decrease in light reflectance), and a brightening (an increase in light reflectance), of the retina, were measured. Under infrared observation, the light reflectance of the whole posterior retina decreased (the fundus image became darker) after a flash stimulus (Fig. 1B). The optical signal was calculated as follows: (1) the gray-scale values of the image obtained after the

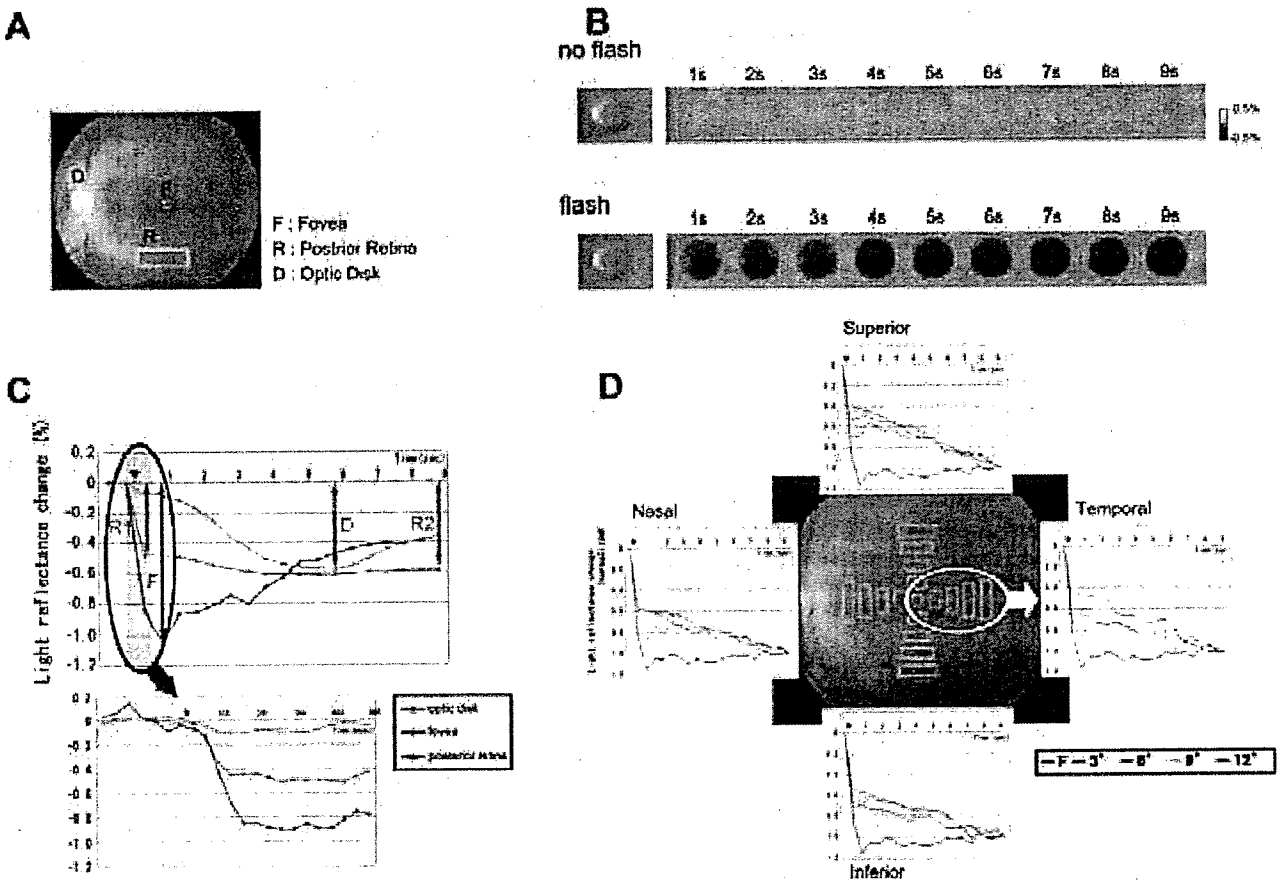

FIGURE 1. Fundus photograph and time courses of intrinsic signals after a flash stimulus. (A) Fundus photograph of normal retina showing the regions analyzed. (B) Time courses of two-dimensional images of ocular fundus showing the light reflectance changes during a 10-second trial without (*top*) and with (*bottom*) a flash stimulus. *Left*: fundus images taken at the beginning of a trial; *right*: light reflectance changes after a flash. Thirty consecutive video frames collected during 1 second were averaged for one poststimulus fundus image. Darkened regions indicate a decrease of light reflectance after the flash stimulus. (C) Plot of the time courses of light reflectance changes in a single trial after a diffuse flash stimulus in the three locations shown in (A). The time after the flash is shown on the abscissa. *Arrowhead*: point of delivery of the flash. Each point is the average of 15 video frames collected during 0.5 second of the light reflectance changes. *Colored arrows*: **F** signal at fovea, **D** signal at the optic disc and **R1** and **R2** signals in the nonfoveal posterior retina. The time course of the reflectance changes during the first 500 ms after a flash is shown in the *bottom* graph where each point is the average of two video frames during one-fifteenth of a second. (D) Time courses of light reflectance changes in a single trial after a diffuse flash, measured at the fovea and four different regions within 12° from the fovea in each quadrant. Amplitudes are indicated as values relative to the light reflectance changes at the end of each trial (1.0). The four regions tested in each quadrant are indicated as distances from fovea (3°, 6°, 9°, and 12°).

COLOR

stimulus were divided, pixel by pixel, by those obtained during a 0.5-second period before the stimulus, and (2) this ratio was rescaled to 256 levels of gray-scale resolution to show the stimulus-induced reflectance changes.

A deterioration of the signal can be caused by movement artifacts: small involuntary eye movements, blood pressure pulsations, and respiration-associated movements. Eye movements are the most serious artifacts because a different fundus position would be analyzed during the pre- and poststimulus periods. However, these artifacts can be minimized by giving sufficient amounts of muscle relaxants to block eye movements. Pulsations cause small movements of the retinal arteries and optic disc. However, the pulsation-derived reflectance changes are less than one tenth of the stimulus-induced reflectance changes and are almost negligible if 15 video frames are averaged during the 0.5 seconds (Fig. 1C).

Artifacts from respiratory movements produced large light reflectance changes, which were 20% to 40% of the stimulus-induced reflectance changes. This artifact is due to changes in blood flow or volume and periodic back-and-forth movement of the eye, synchronized with the respiration. In our recordings, the respiration-induced artifacts were significant, and the respirator had to be stopped during a recording period of 10 seconds. With the respirator stopped, we could record stable intrinsic signals whose quality was sufficient to map the retinal reflective changes in a single trial without either averaging or offline analysis with realignment of the images.[6]

To measure the time course of the signal changes, we recorded two trials under the same conditions and averaged the results. We found that each trial had to be recorded with at least a 20-minute interval to allow a recovery of the signal production from the previous stimulus. Thus, in experiments where the 11 stimulus intensities were recorded, up to 7 to 8 hours were necessary to record two trials under each condition. Because only two recordings were obtained under each recording condition, the type of statistics that could be used was limited. Unlike ERG recordings, the amplitudes of intrinsic signals are vulnerable to changes in the heart rate, blood pressure, and corneal reflectance. Because it is critical for quantitative comparisons to measure the responses under the same physiological conditions, averaging many trials was impractical for our experimental protocol.

Electroretinograms

A bipolar contact lens electrode (Mayo, Aichi, Japan) was used to record the ERGs. The ERGs were amplified ×10,000 and the band-pass filters were set at 0.3 to 500 Hz (Power Lab; AD Instruments, Colorado Springs, CO). A 45° brief white xenon flash stimulus was delivered through the same observation optical system to stimulate the retina while the fundus was monitored with the infrared observation light. As in intrinsic signal imaging, two ERGs were recorded for each recording condition and were averaged.

Recording Conditions

Initially, we compared the responses of the intrinsic signal images and the ERGs evoked by the same diffuse flash stimulus under different recording conditions: (1) flash intensities (Supplementary Fig. S1; all supplementary figures are online at [INSERT URL]), (2) flash intervals (Supplementary Fig. S2), and (3) background luminance (Supplementary Fig. S3). Second, we stimulated the retina focally and measured the intrinsic signals in the stimulated and nonstimulated regions.

Flash Intensity. The maximum intensity of the xenon flash was 308.0 cd · s/m^2, and neutral density filters were used to attenuate the intensity. The intrinsic signals and ERGs were recorded over an 8.8-log-unit range in 11 steps (−8.8, −7.8, −6.7, −6.0, −4.8, −3.7, −3.0, −1.8, −0.7, −0.3, and 0.0). The recordings were performed consecutively with 20 minutes between changes in the intensity under both the dark- and light-adapted conditions. In the light-adapted condition, each recording was followed by 10 minutes of light adaptation. For light adaptation, an 80-mm diameter white polyethylene ball, similar to a ping-pong ball, was cut in half and placed between the fundus camera and the eye. The ball was illuminated by two halogen lamps through fiber optics so that the luminance in the center was 30 cd/m^2. Although the luminance of the ball was not spatially uniform, we believe, that this did not affect the results of the experiments significantly because the luminance at 10° from the center varied by only 94.4% to 103.0% relative to the center (100%). The illuminated ball was removed a few seconds before each recording trial.

Flash Intervals. The intrinsic signals and ERGs were recorded after 0.5, 1.0, 3.0, 5.0, 10, 30, and 60 minutes of flash-to-flash intervals. After a 30-minute recovery period, the posterior retina was first bleached by a strong white flash stimulus (bleaching flash: −0.3 log units: 1.54×10^2 cd · s/m^2), followed by the various interval times listed. The intrinsic signals and ERGs were then measured with a flash (recording flash) of the same intensity as the bleaching flash.

Background Luminance. The background luminance was changed from 0 to 200 cd/m^2 in five steps, to examine the effects of background luminance on the intrinsic signal images. For the intrinsic signal imaging, a strong white flash (−0.3 log units: 1.54×10^2 cd · s/m^2) was used as a stimulus. For the ERGs, the flash intensity, that evoked the maximum b-wave (−3.0 log: 3.08×10^{-1} cd · s/m^2) was used.[17] Each recording trial was recorded with a 20-minute interval.

Finally, a focal stimulus was projected onto the retina by inserting a transparent film in the optical pathway of the Xenon strobe. The film was placed at a point that was conjugate to the retina. The shape and size of the stimulus on the retina was determined by the pattern on the film.

Results

The time course of the intrinsic signals evoked by a brief flash stimulus was different for different regions of the ocular fundus. A representative flash-evoked response from a single trial under dark-adapted condition is shown in Figure 1C. The reflectance changes at the fovea were rapid and reached a negative peak (darkening) within 100 to 200 ms after the flash. The darkening then gradually returned to the prestimulus baseline. The changes in the signals at the optic disc were much slower and reached a peak 5 to 6 seconds after the flash. The signals in the nonfoveal posterior retina were composed of both fast and slow components. The light reflectance decreased rapidly within 100 ms (flexural point) and then gradually decreased, reaching a trough 5 to 6 seconds after the flash. As shown in Figure 1D, the time course of the intrinsic signals of the posterior retina was approximately the same over the whole field except for the small central region within the avascular foveal area (i.e., 300 μm in diameter).[18] The light reflectance at the fovea did not decrease after the initial negative peak.

There is some evidence that the signal in the nonfoveal posterior retina is composed of at least two components. First, the threshold of the fast and slow signals were different by 4 log units of flash intensity in the dark-adapted condition and 1 or 2 log units in the light-adapted condition, as shown by the following results. Only the later phase of the slow reflectance change was observed after a dim flash stimulus. Second, only the amplitude of the late phase of the signal is vulnerable to changes in the heart rate, whereas that of the early phase is not changed (see the Discussion section).

To analyze the flash-induced intrinsic signals and electrophysiological responses, we used the value of the initial peak of light reflectance change at the fovea (**F**: 15 × 15 pixels), the value at the flexural point of light reflectance change (**R1**), or the value at the end of the recording trial (**R2**) in the inferior retina (60 × 40 pixels), and the lowest value of light reflectance at the optic disc (**D**: −70 × 50 pixels; Fig. 1C). AQ: 3

taprald4/z7g-lovs/z7g-lovs/z7g00507/z7g8167d07a | moyerr | S=11 | 3/6/07 | 19:07 | Art: 06-1294 | Input-mr

Stimulus Intensity

The intrinsic signal images and ERGs recorded after a diffuse flash are shown in Figures 2A, 3A, 4A, and 5A, and the intensities of the intrinsic signals and ERG amplitudes are shown in Figures 2B, 3B, 4B, and 5B.

F2 Under dark-adapted conditions (Fig. 2), the amplitudes of a- and b-waves of the ERGs increased as the stimulus intensity increased.[19] The intrinsic signals of **D** and **R2** had the same threshold as that of the b-wave, and their amplitudes also increased as the intensity increased. The amplitudes of **D** and **R2** reached a plateau at −6.0 log units and did not change significantly with higher intensities. **R2** increased again with higher flash intensities over −0.3 log unit in monkey (M)1 and −0.7 log unit in M2.

The threshold of **R1** was higher than that of **D**, **R2**, and the ERG a-wave. The amplitude of **R1** increased gradually with increasing flash intensities. The amplitude of **F** also increased with increasing flash intensities, but its threshold was higher than that of any of the other intrinsic signals.

Under light-adapted conditions (30 cd/m^2), the amplitudes of the a- and b-waves increased progressively with increasing flash intensities, but that of the b-wave decreased with intensities higher than −3.0 log units, due to the photopic hill

F3 phenomenon (Fig. 3).[17] The thresholds of **D** and **R2** of the intrinsic signal images were higher than those in the dark-adapted condition by 2.1 log units in M1 and 2.8 log units in M2. The thresholds of the **D** and **R2** signals and ERG a- and b-waves were the same in M1.

The threshold of **R1** was the same in both dark- and light-adapted conditions. In both conditions, the threshold of **F** was the same in M1 but was 0.7 log unit lower than that in M2 in the dark-adapted condition. What was striking was that the amplitude of **R2** was smaller with brighter flashes in M2 under light-adapted conditions and the light reflectance change became approximately zero at −0.3-log-unit intensity. There was a tendency for the amplitude of the **R2** signal to decrease with intensities that were 1.0 to 2.0 log units higher than the threshold of the **R1** signal.

Effect of Changes in Flash Intervals

After a bleaching with a bright flash, the amplitudes of the a- and b-waves were reduced and the amplitudes increased with increasing time in the dark (Fig. 4).[20,21] The recovery of the F4 ERG amplitudes appeared slower than that in other studies because our flash intensity was 1.7 log units more intense than that of the ISCEV (International Society for Clinical Electrophysiology of Vision) standard flash.

For the intrinsic signals, only the **F** signal had a pattern similar to that of the ERGs (i.e., the amplitude increased gradually with longer intervals in the dark after the preceding flash). **D**, **R1**, and **R2** had peaks at 3 to 5 minutes after the preceding flash, and the amplitudes decreased at 10-minute intervals. These findings indicate that the source of the intrinsic signals of the optic disc and the nonfoveal posterior retina are different from that of the fovea.

Effect of Background Luminance

The amplitudes of the a- and b-waves decreased progressively as the background illumination increased (Fig. 5).[22,23] The F5 amplitudes of **D** and **R1** of the intrinsic signals under light-adapted conditions (10–200 cd/m^2) were 45% to 65% as large as that in the dark-adapted condition in M1 and 60% to 80% in M2. The amplitude of **F** in the light-adapted condition was approximately 90% as large as that in dark-adapted condition in M1 and 80% to 100% in M2.

In contrast, the **R2** signal, was markedly decreased under light-adapted conditions. Even with a weak background of 10 cd/m^2, **R2** was decreased by approximately 90% in M2, and an increase of 20% in light reflectance was observed in M1. This

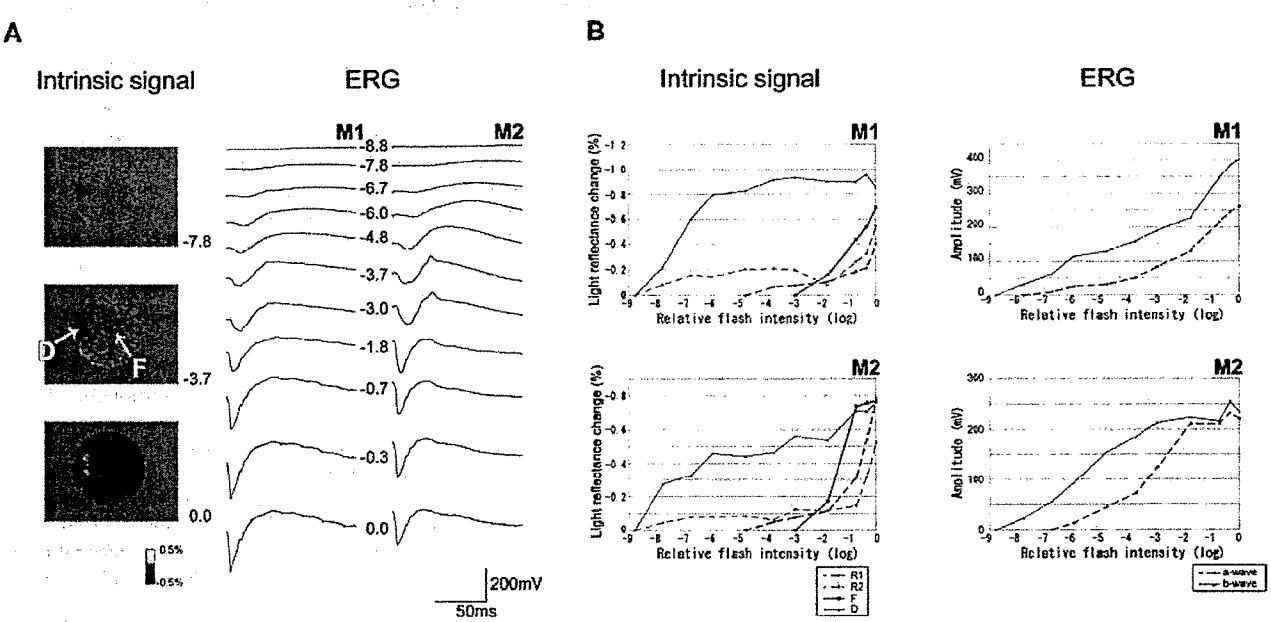

FIGURE 2. Intrinsic signal images and ERGs after a diffuse stimulus in dark-adapted conditions. (A) Fundus images of the intrinsic signals (*left*) and ERGs (*right*) after a diffuse flash in the dark-adapted condition with stimulus intensities from −8.8 to 0 log units. *Left*: intrinsic signal images from a single trial averaged from 5.0 to 8.0 seconds after the flash. The darkened region in fundus images indicates light reflectance decrease after the flash. The ERGs recorded from monkeys M1 and M2 are shown. The relative log flash intensity responses to the maximum flash are indicated. D: optic disc, F: fovea. (B) *Left*: amplitudes of **R1**, **R2**, **F**, and **D** of the intrinsic signals in response to increasing flash intensities are shown as light reflectance changes for M1 and M2. *Right*: the amplitudes of the ERG a- and b-waves in response to the same stimulus series. Note that negative values of light reflectance changes are plotted to indicate the strength of intrinsic signals.

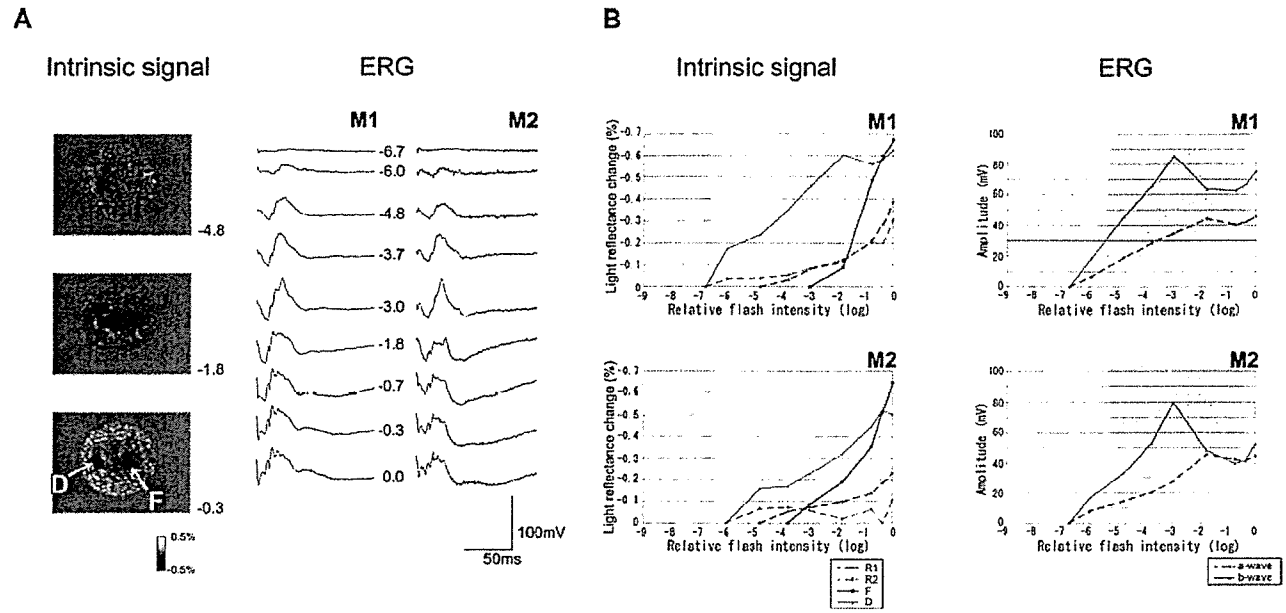

FIGURE 3. Intrinsic signals and ERGs after a diffuse stimulation under light-adapted conditions. (**A**) Fundus images of the intrinsic signals (*left*) and ERGs (*right*) after different stimulus intensities (−6.7–0 log-unit intensity). Representative signal images for a single trial averaged from 5.0 to 8.0 seconds after a flash are shown. (**B**) Amplitudes of **R1**, **R2**, **F**, and **D** of the intrinsic signals and the a- and b-waves of the ERGs in response to various flash intensities are as described in Figure 2.

means that the posterior retina appeared brighter after a flash at the later phase of a recording trial with bright background illumination.

Responses at Optic Disc

We have shown that the thresholds of the light reflectance changes at the optic disc were comparable to the threshold of the ERG b-waves and that even a dim stimulus can evoke a strong signal at the optic disc (Fig. 2). To determine the contribution of blood-related changes to the intrinsic signals at the optic disc, we measured the responses from different regions within the optic disc (Fig. 6A): (1) the central region where the central retinal artery and vein run perpendicular to the imaging plane (Center), (2) over the superior branch of the central retinal artery (Artery), (3) over the superior branch of the central retinal vein (Vein), (4) temporal and nasal regions

F6

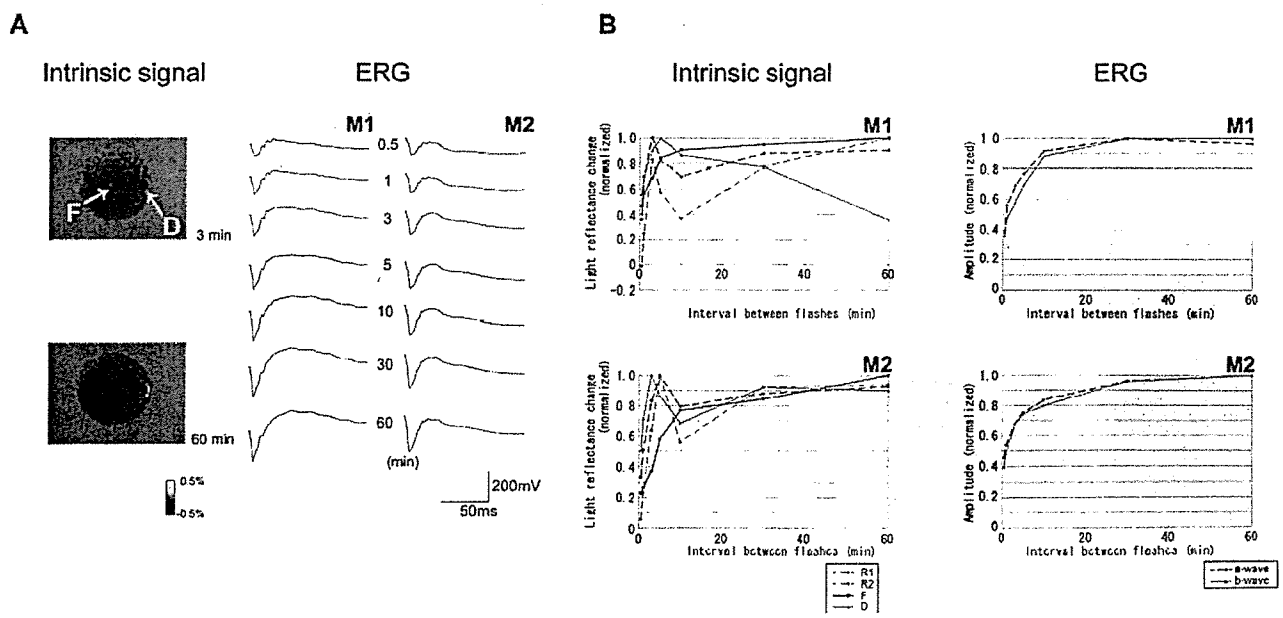

FIGURE 4. Intrinsic signals and ERGs after a diffuse stimulus recorded at different times after bleaching. (**A**) Fundus images of intrinsic signals (*left*) and ERGs (*right*) evoked by a diffuse flash (−0.3 log unit) at different intervals (0.5–60 minutes) after a bleaching flash at the same intensity. Representative images from a single trial averaged from 5.0 to 8.0 seconds after a flash are shown. (**B**) Amplitudes of **R1**, **R2**, **F**, and **D** of the intrinsic signals and a- and b-waves of the ERGs at different flash intervals. Amplitudes are relative to the maximum for each signal component.

tapraid4/z7g-iovs/z7g-iovs/z7g00507/z7g8167d07a | moyerr | S=11 | 3/6/07 | 19:07 | Art: 06-1294 | Input-mr

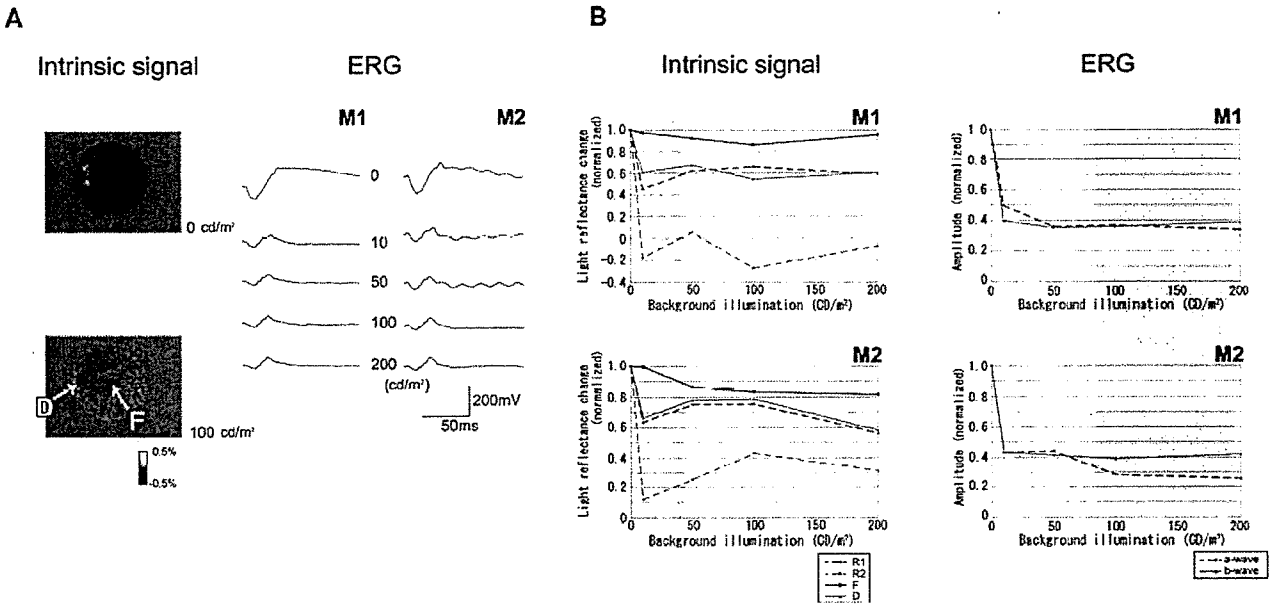

FIGURE 5. Intrinsic signal images and ERGs after a diffuse flash stimulus on different background luminances. (A) Fundus image of intrinsic signals (*left*) and ERGs (*right*) after a diffuse flash on different background luminances (0–200 cd/m^2). Representative signal images in a single trial averaged from 5.0 to 8.0 seconds after a flash (−0.3 log unit) are shown. For the ERGs, a flash with the maximum intensity which evoked a b-wave without photopic hill phenomenon was used (−3.0 log units). (B) Amplitudes of **R1**, **R2**, **F**, and **D** of the intrinsic signals and the ERG a- and b-waves with different background luminances. Amplitudes are relative to the maximum for each signal component.

where large vessels are not present (Temporal and Nasal), and (5) the entire optic disc (D). A diffuse flash of −0.7 log unit intensity was used for stimulation, and 17 consecutive trials with 3-minute intervals were averaged.

The light reflectance changes were especially large in the central region where the central retinal artery and vein pass through the optic nerve (three times larger than that in the whole region; Fig. 6B). The light reflectance changes over the superior branch of the central retinal artery and vein were 1.2 times larger than that of the whole region. Although the size of the intrinsic signals varied in different regions within the margins of the optic disc, the time course at each region seemed to be almost the same (Fig. 6C).

Focal Stimulation

The recording of the focal macular ERG is a technique used to measure the electrical responses in the macula by focally stimulating the macular region.[24,25] Focal flash stimuli can be given to the posterior retina with our recording system, however, our system is not setup to deliver a background illumination to suppress the rod responses and cannot measure the electrical activity in the stimulated region. We have stimulated focal regions of the posterior retina, and compared the time course of the intrinsic signals in both the stimulated and nonstimulated regions in dark-adapted conditions.

First, the macular area including the fovea was focally stimulated with an 8.8° circular stimulus (Figs. 7A, 7B). The light F7

COLOR

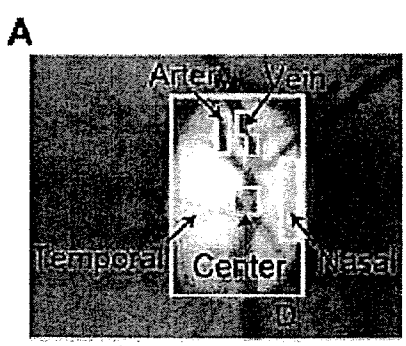

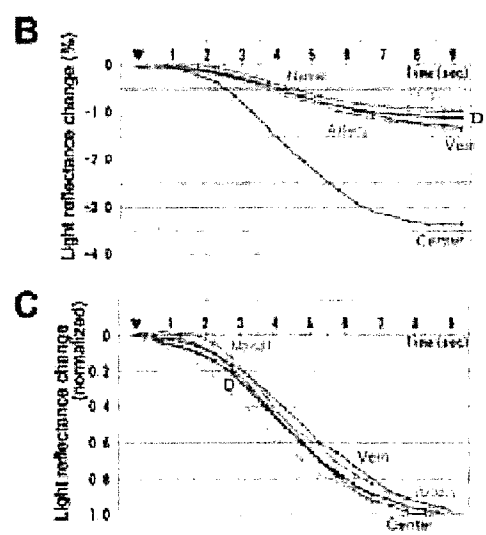

FIGURE 6. Time courses of intrinsic signals evoked by a diffuse flash from six regions of the optic disc. (A) Photograph of the optic disc showing the areas measured. D, entire optic disc; Center, central region where central retinal artery and vein run perpendicularly to the imaging plane; Artery, superior branch of central retinal artery; Vein, superior branch of central retinal vein; Temporal, temporal region, where large vessels are not present; and Nasal, nasal region, where large vessels are not present. (B) Plot of the time courses of the intrinsic signals measured at the six regions of the optic disc, presented as absolute values in light reflectance changes. (C) Plot of the time courses of the intrinsic signals, presented as relative to the maximum for each recording region.

taprald4/z7g-lovs/z7g-lovs/z7g00507/z7g8167d07a | moyerr | S=11 | 3/6/07 | 19:08 | Art: 06-1294 | Input-mr

COLOR

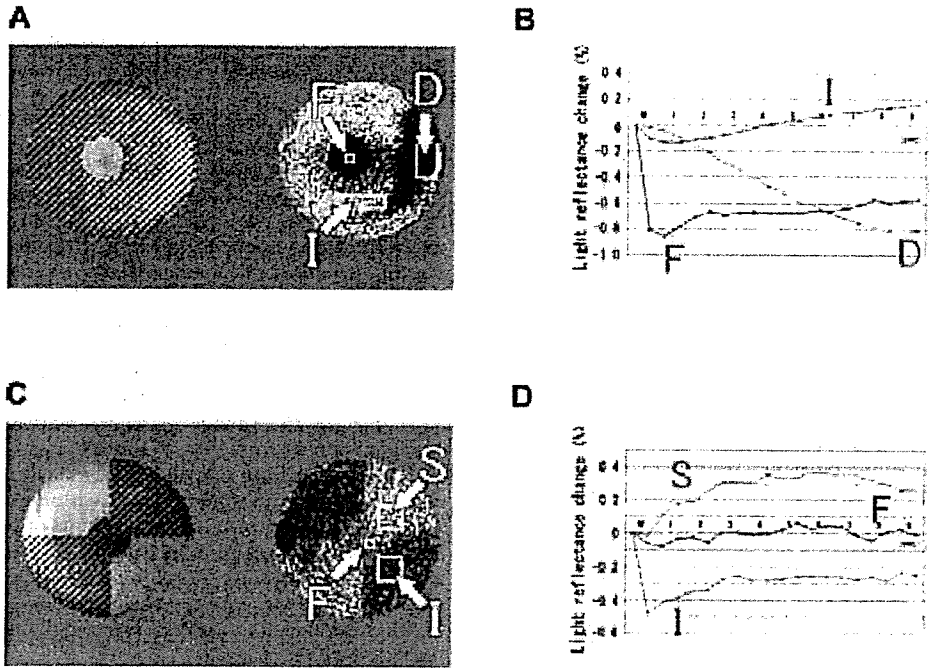

FIGURE 7. Effect of focal stimulus on the intrinsic signals. (**A**) *Left*: fundus image showing circular focal stimulus in the macula including the fovea (8.8° in diameter). The stimulus was blocked over the *hatched area*. Regions for time course analysis are indicated as F (fovea), D (optic disc), I (inferior retina within the vascular arcade, sparing thick vessels). *Right*: fundus image of intrinsic signal evoked by the focal stimulus, averaged from 6.5 to 9.5 seconds after stimulation. Data from four consecutive trials were averaged. (**B**) Plot of the time courses of light reflectance changes in a single trial after a focal flash at the three locations shown in (**A**). (**C**) *Left*: fundus image showing mosaic-like focal stimulus in the posterior pole, sparing central 8.0° including fovea. Regions for time course analysis are indicated as F (nonstimulated fovea), S (stimulated superior retina), and I (nonstimulated inferior retina). Right: two-dimensional image of intrinsic signal evoked by the focal stimulus, averaged from 6.5 to 9.5 seconds after stimulation (single trial). (**D**) Plot of the time courses of light reflectance changes in a single trial after a focal flash at the three locations shown in (**C**).

reflectance in the stimulated region decreased (Fig. 7B; F) and the region that darkened exactly matched the location of the stimulus (Fig. 7A). In contrast, the region without stimulation became brighter at the later phase of a recording trial (Fig. 7B; I). When two quadrants of the posterior retina were stimulated with the macula spared, the intrinsic signal showed exactly the same darkening pattern as the shape of the stimulus (Fig. 7C). The stimulated posterior retina (I) showed a negative R1 and negative R2 signal (i.e., a darkening; Fig. 7D). The nonstimulated area of the posterior pole (S) was brighter (positive R2), which is usually not observed under other recording conditions. The fovea (F), where the stimulus was masked, did not show any light reflectance changes after the flash.

Discussion

The origin of the intrinsic signals in the cerebral cortices has been extensively investigated; however, most of the studies have dealt with the deoxygenation of hemoglobin.[8,9,11] The standard hypothesis is that the intrinsic signals in the cerebral cortex arise from light reflectance changes due to the many metabolic changes after neural activation. For example, the intrinsic signal measured at 570 nm is dominated by changes in the blood volume in the capillaries; That at 600 to 650 nm is dominated by the changes in the deoxygenation level of hemoglobin, and that in the infrared region is dominated by changes in tissue light scattering. Although different metabolic changes are highlighted at different wavelengths, the optical responses obtained at these wavelengths had nearly the same spatial pattern of activation as that of the activated neurons.[9,26] Whatever wavelength was chosen for the measurement of reflectance, the most critical premise for evaluating the intrinsic signal has been that it is the darkening (i.e., a decrease in light reflectance), that correlates with the local neural activity. This is more or less true of the intrinsic signal images in the retina[3]; however, the spatial distribution of the signals appeared to be more complicated when the retina is focally stimulated.

Our goal was to find out what each signal component represented by comparing the intrinsic signals with the ERGs recorded under the same conditions. Although the spatially localized responses of the intrinsic signals cannot be directly compared with the responses in full-field ERGs, this comparison may provide us with some keys to determine the possible mechanisms of the production of the intrinsic signals, because the neuronal mechanisms of the production of the ERGs have been well investigated.

It is important to understand that, in principle, the intrinsic signals are not necessarily produced by photoreceptors: There may be differences in the site of the photoreceptor and the site for producing the signals. The light reflectance changes reflect the summation of the stimulus-evoked metabolic changes happening in the 10 retinal layers, each of which may produce signals with different characteristics. The same difficulty arises when the origin of the different components of the ERGs is investigated. Thus, the type of activated photoreceptors and

the location where the signal is produced should be carefully separated.

D Signals

The threshold of the **D** signal was comparable to that of the ERG b-wave in the dark-adapted condition (Fig. 2).[19] The threshold was higher by 2.0 to 3.0 log units under light-adapted conditions (Fig. 3),[17] and the amplitude was greatly decreased in the presence of background illumination (Fig. 5).[22,23] These results indicate that the **D** signal evoked by a dim flash (weaker than −5.0 or −6.0 log units) under dark-adapted conditions reflects the activation of rod photoreceptors, and those evoked by stronger flash reflects the activation of both cone and rod photoreceptors. The **D** signal evoked under light-adapted conditions reflects mainly the activation of the cone photoreceptors.

The time course of the **D** signal is slow and is probably produced by a flash-induced blood volume or flow increase. The decrease in light reflectance is due to the increased light scattering of the red blood cells. Previous studies have shown that flashing lights can increase the blood flow at the optic disc of humans and cats.[27,28] An increase in blood volume is known to decrease the reflectivity of tissues due to the increased scattering of light by the red blood cells in the blood vessels.[11,29] Although a change in the blood volume or flow was not directly measured in this study, the results of measurements of the intrinsic signals on the optic disc support this (Fig 6). In the central region of the optic disc occupied by the central retinal artery and vein, the reflectance changes were three times greater than in other regions, although the time course was almost the same as at any locations within the optic disc. The light-scattering changes induced by changes in the blood volume or flow may be most effectively observed when the vessels are perpendicular to the imaging plane. Even in the white regions (Fig. 6A, Temporal and Nasal), where large vessels are not present, the light reflectance changes showed a time course similar to that in the central region (Fig. 6C) indicating that this signal is derived from the blood volume or flow changes in the capillaries. As for the question of whether the blood volume or flow contributes more significantly to this signal, we do not have any evidence to conclude which has the greater role and recommend that the mechanism of blood-related light scattering changes be thoroughly investigated.

Neural activity in the optic nerve causes shrinkage of the extracellular space due to cellular swelling, and this was detected optically by intrinsic signal imaging in rats.[30,31] We believe that part of the scattering changes may be due to swelling of the axons of the ganglion cells or of the glial cells. Its contribution to the whole intrinsic signal, however, may be masked by the relatively large reflectance changes due to changes in blood volume or flow. A contribution by the changes in deoxygenated hemoglobin concentration in the capillaries to the intrinsic signal may also exist, although it is believed to be negligible compared with that of tissue light scattering under infrared light observation.[9,11]

R2 Signals

The properties of the **R2** signal were similar to those of the **D** signal, except that **R2** became very small and in some cases became positive under light-adapted conditions (Figs. 3B, 5B). The **R2** signal is probably a complex of different components and origins because the posterior retina is a complex layered structure, and its signal properties cannot be explained simply by the blood volume or flow changes in the capillaries.

We suggest that the inner retina may be the main contributor to the **D** and **R2** signals because this type of slow signal was not observed at the fovea, which lacks the inner retinal layers including the blood vessels.[18] Our data did not allow us to determine which type of cells contribute the most to the flash-evoked responses observed at the optic disc or the posterior retina.

We attempted to keep the systemic condition of the anesthetized monkeys as constant as possible during the data acquisition. In some trials, however, the heart rate became unstable and rapid changes occurred during consecutive recordings under the same stimulus conditions. For example, the heart rate increased from 120 per minute to 140 per minute during two consecutive trials in one monkey. Although such data obtained under unstable conditions were discarded, we did note that it was always the amplitudes of **D** and **R2** signals that were affected by the changes in the heart rate. In contrast, the amplitudes of **F** and **R1** signals were much less affected by changes in heart rate (data not shown). This observation suggests that the **D** and **R2** signals are related to blood-induced changes more than are the **F** and **R1** signals.

It was interesting that the amplitudes of **D** and **R2** signals were largest with 3- to 5-minute flash intervals (Fig. 4B). This finding is very different from the results of ERGs. It is possible that the mechanism by which neural activity is converted to the vascular response (i.e., neurovascular coupling)[32,33] is most effectively activated when the stimuli are given repeatedly at intermediate intervals. This possibility should be investigated more extensively.

F Signals

The **F** signal, which is the average of light reflectance changes within the central 300 μm in diameter was faster than the **D** and **R2** signals and reaches its peak within 100 to 200 ms (Fig. 1C). The threshold for the **F** signal was much higher than any other signals and was the same in both dark- and light-adapted conditions. The characteristic anatomic structure of the fovea (viz., the absence of rod photoreceptors, capillaries and other inner retinal layers), indicates that the **F** signal reflects the activation of cone photoreceptors under any recording conditions.

The light-scattering changes due to the microstructural changes after activation of the cone photoreceptors are probably the source of the **F** signals because the foveal avascular region is free of capillaries and not subject to the changes in hemoglobin concentration or blood volume after neural activation.[18] Recent functional OCT studies using blood-free slice preparations showed that the reflectance in the photoreceptor layer is strongly changed by neural activation followed by microscopic morphologic changes.[34,35]

R1 Signals

The amplitude of the **R1** signal increases with an increase in stimulus intensity under both dark- and light-adapted conditions as did the **F** signal. The threshold of **R1** lies between the threshold for the optic disc and fovea and was the same under both dark- and light-adapted conditions. This leads us to think that cone photoreceptors mainly contribute to the **R1** signal, because bleaching of rods in the bright condition did not change the **R1** threshold. It is difficult to assume, however, that rod and cone photoreceptors play different roles in light reflectance changes.

The property of the **R1** signal is complicated in another way. The abrupt darkening after a flash may well be explained by the photoreceptor responses like the **F** signal, but the results in Figure 4B strongly suggest that **R1** share the same signal origin with **D** and **R2** signals: The amplitude of **R1** signal did not increase with longer interstimulus intervals, but attained a maximum with 3- to 5-minute intervals as with the **D** and **R2** signals. We suggest that the **R1** signal is produced not

TABLE 1. Properties of Four Components in Retinal Intrinsic Signals

	Signal Components			
	D	F	R1	R2
Time to the peak in amplitude	Slow	Fast	Fast	Slow
Threshold in dark adaptation (log unit) (ERG a-wave, −6.7; b-wave, −7.8)	−7.8	−1.8	−4.8	−7.8
Threshold shift in light adaptation	++	−	±	++
Increase in amplitude with shorter flash intervals (3–5 min)	+	−	+	+
Decrease in amplitude by light adaptation	+	±	+	++
Possible sources				
Contribution of blood-related light reflectance changes	++	−	?	++
Contribution of inner or middle layer	++	−	+?	+
Contribution of outer layer	−	++	+?	+?

only by photoreceptors but also by other inner or middle layer structures, although our data do not provide any evidence for the exact origin.

A summary of the various properties in four signal components is shown in Table 1.

Focal Stimulation

Focal stimulation of the retina is one way to evaluate local neural activity in a dysfunctional retina and has been applied clinically with the focal macular ERG.[24,25] The intrinsic signals measured with focal stimuli showed that this technique can also be used to study focal responses. The focally stimulated region showed a decrease in the light reflectance after the stimulus, and this darkened region exactly matched the location of the focal stimulus (Figs. 7A, 7C). It was striking that the nonstimulated posterior pole showed a slow light reflectance increase after a fast light reflectance decrease (Fig. 7B; I). In another case, the nonstimulated posterior pole showed only a light reflectance increase (Fig. 7D; S).

The brightening observed in the nonstimulated region in later phase (Fig. 7B, I; Fig. 7D; S) may be explained by (1) some type of horizontal interaction by, for example, horizontal cells, through which stimulated neurons could affect the reflectivity of the neurons outside the stimulated region, or (2) the spatial interaction in the intrinsic signals between the stimulated and nonstimulated regions via an inhomogeneous distribution of capillary blood flow.[8,9,11,56] These explanations, however, do not account for the strong and homogeneous brightening over the whole posterior region triggered by a small focal stimulus.[37] It is possible that the properties of the signals, such as polarity and threshold, are different in different retinal layers, and the difference in signal time course between stimulated and nonstimulated regions would reflect the difference of layers that mainly contribute to the light reflectance changes.

Recently, OCT imaging of neural activity has been demonstrated in the feline visual cortex,[38] isolated frog and rabbit retina,[54,55] and intact rat retina.[39] Functional OCT studies in slice preparations have revealed the complex nature of flash-evoked changes in the reflectances from various intraretinal layers: a decrease of near infrared scattering in the photoreceptor layer and an increase in the ganglion cell layer,[54] or a decrease in the photoreceptor inner segment and increase in the internal plexiform layer and photoreceptor outer segments.[55] Srinivasan et al.[39] first reported the results of functional OCT signals in the intact retina and demonstrated the flash-evoked reflectance increase in the photoreceptor outer segments. In these studies, the increase in light reflectance after a flash was mainly observed in the photoreceptor layer, whereas the decrease was mainly observed in monkey and human retinas.[5,6] This difference in signal polarity may be attributable to the difference in the methods used to measure the reflectances. In addition, other factors, such as the use of sectioned preparations that lack the RPE layer and blood supply, differences among species, and differences in the recording region in the retina, should also be considered.

The light-scattering changes after a flash observed in functional OCT is thought to be derived from the structural changes in the outer segment discs, membrane hyperpolarization, cell swelling, and changes in the composition of the interphotoreceptor matrix.[54,55] These sources can also explain the rapid light reflectance changes (F and R1) observed in our study. As suggested by our results and those of functional OCT studies of retinal sections, the characteristics of the light reflectance changes after a flash are different in different layers and different retinal locations and may be far more complex than the conventional idea of intrinsic signals mainly investigated in the cerebral cortex.[8,9,11] Interpretation of the retinal intrinsic signal is thus difficult, and maximum care should be taken in choosing the proper recording conditions and which signal is most closely correlated with the neural activities of the retina.

In conclusion, our results showed that the intrinsic signals in the retina are composed of several components of different origins, although the precise cellular mechanisms of signal production were not determined. The sensitivity of intrinsic signal images was high enough to detect weak neural activity in the retina (e.g., the slow signals in the posterior retina and the optic disc were as sensitive as the ERG b-wave in the dark-adapted condition). Moreover, the distribution of intrinsic signals reflects not only the cellular distribution in the retina but the current level of the activities. Although the source of the signal was much more complex than initially thought, by carefully selecting the proper recording condition, this imaging technique may have a potential to estimate the neural responses of different origins and obtain more useful information about various types of retinal disorders with different etiologies than the conventional electrophysiological examinations such as full-field ERGs, focal macular ERGs, and multifocal ERGs.

Acknowledgments

The authors thank Uma Maheswari Rajagopalan for critical comments on the manuscript.

References

1. Huang D, Swanson EA, Lin CP, et al. Optical coherence tomography. *Science*. 1991;254:1178–1181.
2. Hee MR, Izatt JA, Swanson EA, et al. Optical coherence tomography of the human retina. *Arch Ophthalmol*. 1995;113:325–332.
3. Tsunoda K, Oguchi Y, Hanazono G, Tanifuji M. Mapping cone- and rod-induced retinal responsiveness in macaque retina by optical imaging. *Invest Ophthalmol Vis Sci*. 2004;45:3820–3826.

4. DeLint PJ, Berendschot TT, van de Kraats J, van Norren D. Slow optical changes in human photoreceptors induced by light. *Invest Ophthalmol Vis Sci.* 2000;41:282–289.
5. Nelson DA, Krupsky S, Pollack A, et al. Special report: Noninvasive multi-parameter functional optical imaging of the eye. *Ophthalmic Surg Lasers Imaging.* 2005;36:57–66.
6. Abramoff MD, Kwon YH, Ts'o D, et al. Visual stimulus-induced changes in human near-infrared fundus reflectance. *Invest Ophthalmol Vis Sci.* 2006;47:715–721.
7. Critin M, Riva CE. Functional imaging of the human papilla and peripapillary region based on flicker-induced reflectance changes. *Neurosci Lett.* 2004;360:141–144.
8. Frostig RD, Lieke EE, Ts'o DY, Grinvald A. Cortical functional architecture and local coupling between neuronal activity and the microcirculation revealed by in vivo high-resolution optical imaging of intrinsic signals. *Proc Natl Acad Sci USA.* 1990;87:6082–6086.
9. Malonek D, Grinvald A. Interactions between electrical activity and cortical microcirculation revealed by imaging spectroscopy: implications for functional brain mapping. *Science.* 1996;272:551–554.
10. Tsunoda K, Yamane Y, Nishizaki M, Tanifuji M. Complex objects are represented in macaque inferotemporal cortex by the combination of feature columns. *Nat Neurosci.* 2001;4:832–838.
11. Pouratian N, Toga A. Optical imaging based on intrinsic signals. In: Toga AW, Mazziotta JC, eds. *Brain Mapping.* San Diego, CA: Academic Press; 2002:97–140.
12. Bowmaker JK, Dartnall HJ, Mollon JD. Microspectrophotometric demonstration of four classes of photoreceptor in an old world primate, Macaca fascicularis. *J Physiol.* 1980;298:131–143.
13. Bowmaker JK, Dartnall HJ. Visual pigments of rods and cones in a human retina. *J Physiol.* 1980;298:501–511.
14. Kilbride PE, Read JS, Fishman GA, Fishman M. Determination of human cone pigment density difference spectra in spatially resolved regions of the fovea. *Vision Res.* 1983;23:1341–1350.
15. Kilbride PE, Alexander KR, Fishman M, Fishman GA. Human macular pigment assessed by imaging fundus reflectometry. *Vision Res.* 1989;29:663–674.
16. Elsner AE, Burns SA, Webb RH. Mapping cone photopigment optical density. *J Opt Soc Am A.* 1993;10:52–58.
17. Wali N, Leguire LE. The photopic hill: a new phenomenon of the light adapted electroretinogram. *Doc Ophthalmol.* 1992;80:335–345.
18. Weinhaus RS, Burke JM, Delori FC, Snodderly DM. Comparison of fluorescein angiography with microvascular anatomy of macaque retinas. *Exp Eye Res.* 1995;61:1–16.
19. Fulton AB, Rushton WA. The human rod ERG: correlation with psychophysical responses in light and dark adaptation. *Vision Res.* 1978;18:793–800.
20. Wagman IH, Waldman J, Naidoff D, Feinschil LB, Cahan R. The recording of the electroretinogram in humans and in animals: investigation of retinal sensitivity following brief flashes of light. *Am J Ophthalmol.* 1954;38:60–69.
21. Mahroo OA, Lamb TD. Recovery of the human photopic electroretinogram after bleaching exposures: estimation of pigment regeneration kinetics. *J Physiol.* 2004;554:417–437.
22. Biersdorf WR, Armington JC. Level of light adaption and the human electroretinogram. *J Opt Soc Am.* 1960;50:78–82.
23. Bui BV, Fortune B. Origin of electroretinogram amplitude growth during light adaptation in pigmented rats. *Vis Neurosci.* 2006;23:155–167.
24. Miyake Y, Horiguchi M, Tomita N, et al. Occult macular dystrophy. *Am J Ophthalmol.* 1996;122:644–653.
25. Miyake Y, Shiroyama N, Horiguchi M, Ota I. Asymmetry of focal ERG in human macular region. *Invest Ophthalmol Vis Sci.* 1989;30:1743–1749.
26. Fukuda M, Rajagopalan UM, Homma R, Matsumoto M, Nishizaki M, Tanifuji M. Localization of activity-dependent changes in blood volume to submillimeter-scale functional domains in cat visual cortex. *Cereb Cortex.* 2005;15:823–833.
27. Riva CE, Harino S, Shonat RD, Petrig BL. Flicker evoked increase in optic nerve head blood flow in anesthetized cats. *Neurosci Lett.* 1991;128:291–296.
28. Riva CE, Falsini B, Logean E. Flicker-evoked responses of human optic nerve head blood flow: luminance versus chromatic modulation. *Invest Ophthalmol Vis Sci.* 2001;42:756–762.
29. Narayan SM, Esfahani P, Blood AJ, Sikkens L, Toga AW. Functional increases in cerebral blood volume over somatosensory cortex. *J Cereb Blood Flow Metab.* 1995;15:754–765.
30. Ransom BR, Yamate CL, Connors BW. Activity-dependent shrinkage of extracellular space in rat optic nerve: a developmental study. *J Neurosci.* 1985;5:532–535.
31. MacVicar BA, Feighan D, Brown A, Ransom B. Intrinsic optical signals in the rat optic nerve: role for K(+) uptake via NKCC1 and swelling of astrocytes. *Glia.* 2002;37:114–123.
32. Roy C, Sherrington C. On the regulation of the blood supply of the brain. *J Physiol.* 1890;11:85–108.
33. Villringer A, Dirnagl U. Coupling of brain activity and cerebral blood flow: basis of functional neuroimaging. *Cerebrovasc Brain Metab Rev.* 1995;7:240–276.
34. Yao XC, Yamauchi A, Perry B, George JS. Rapid optical coherence tomography and recording functional scattering changes from activated frog retina. *Appl Opt.* 2005;44:2019–2023.
35. Bizheva K, Pflug R, Hermann B, et al. Optophysiology: depth-resolved probing of retinal physiology with functional ultrahigh-resolution optical coherence tomography. *Proc Natl Acad Sci USA.* 2006;103:5066–5071.
36. Toth LJ, Rao SC, Kim DS, Somers D, Sur M. Subthreshold facilitation and suppression in primary visual cortex revealed by intrinsic signal imaging. *Proc Natl Acad Sci USA.* 1996;93:9869–9874.
37. Kaplan E, Benardete E. The dynamics of primate retinal ganglion cells. *Prog Brain Res.* 2001;134:17–34.
38. Maheswari RU, Takaoka H, Kadono H, Homma R, Tanifuji M. Novel functional imaging technique from brain surface with optical coherence tomography enabling visualization of depth resolved functional structure in vivo. *J Neurosci Methods.* 2003;124:83–92.
39. Srinivasan VJ, Wojtkowski M, Fujimoto JG, Duker JS. In vivo measurement of retinal physiology with high-speed ultrahigh-resolution optical coherence tomography. *Opt Lett.* 2006;31:2308–2310.

Cerebral Cortex June 2005;15:823-833
doi:10.1093/cercor/bhh183
Advance Access publication September 30, 2004

Localization of Activity-dependent Changes in Blood Volume to Submillimeter-scale Functional Domains in Cat Visual Cortex

Mitsuhiro Fukuda[1,2], Uma Maheswari Rajagopalan[1], Ryota Homma[1], Madoka Matsumoto[1,3], Makoto Nishizaki[1,4] and Manabu Tanifuji[1]

[1]Laboratory for Integrative Neural Systems, RIKEN Brain Science Institute, 2-1 Hirosawa, Wako-shi, Saitama, 351-0198, Japan
[2]Present address: Department of Neurobiology, Brain Imaging Research Center, University of Pittsburgh, 3025 East Carson Street, PA 15203, USA
[3]Present address: Laboratory for Cognitive Brain Mapping, RIKEN Brain Science Institute, 2-1 Hirosawa, Wako-shi, Saitama, 351-0198, Japan
[4]Present address: Advanced Technology Research Laboratories, Matsushita Electric Industrial Co., Ltd., 3-10-1 Higashimita, Tama-ku, Kawasaki-shi, 214-8501, Japan

We have examined whether blood volume changes induced by neural activation are controlled precisely enough for us to visualize the submillimeter-scale functional structure in anesthetized and awake cat visual cortex. To activate the submillimeter-scale functional structures such as iso-orientation domains in the cortex, visual stimuli (gratings) were presented to the cats. Two methods were used to examine the spatial precision of blood volume changes including changes in total hemoglobin content and changes in plasma volume: (i) intrinsic signal imaging at the wavelength of hemoglobin's isosbestic point (569 nm) and (ii) imaging of absorption changes of an intravenously injected dye. Both measurements showed that the visual stimuli elicited stimulus-nonspecific and stimulus-specific blood volume changes in the cortex. The former was not spatially localized, while the latter was confined to iso-orientation domains. From the measurement of spatial separation of the iso-orientation domains, we estimated the spatial resolution of stimulus-specific blood volume changes to be as high as 0.6 mm. The changes in stimulus-nonspecific and -specific blood volume were not linearly correlated. These results suggest the existence of fine blood volume control mechanisms in the capillary bed in addition to global control mechanisms in arteries.

Keywords: cerebral blood flow, functional MRI, hemodynamic response, intrinsic signal imaging, orientation column, spectroscopic analysis

Introduction

The activation of cortical neurons elicits changes in light reflection from an exposed cortical surface. The measurement of these light reflection changes (intrinsic signals) enables cortical functional structures to be visualized at submillimeter-scale spatial resolution and provides profound insights into cortical functions in visual areas (Grinvald *et al.*, 1986; Ts'o *et al.*, 1990; Bonhoeffer and Grinvald, 1991, 1993; Malonek *et al.*, 1994; Roe and Ts'o, 1995; Wang *et al.*, 1996, 1998; Ghose and Ts'o, 1997; Tsunoda *et al.*, 2001).

Circumstantial evidence suggests that hemodynamic responses, such as changes in deoxyhemoglobin (Hbr) concentration and blood volume changes, are the major sources of intrinsic signals at visible wavelengths (Frostig *et al.*, 1990; Bonhoeffer and Grinvald, 1996; Malonek and Grinvald 1996). Decreases in light reflection (i.e. increases in light absorption) at 600–630 nm, where the absorption coefficient of Hbr is 5–10 times higher than that of oxyhemoglobin (HbO_2) (Fig. 1 inset), suggest that increases in Hbr concentration are accompanied by the oxygen consumption of activated neurons (Silver, 1978; Sibson *et al.*, 1998; Thompson *et al.*, 2003). The decrease in light reflection at the wavelength where the absorption coefficient of HbO_2 equals that of Hbr (i.e. hemoglobin's isosbestic point) suggests that an increase in total hemoglobin (Hbt) concentration (blood volume change) is another component of the signal. In addition to these hemodynamic components, activity-dependent light scattering (Ls) changes (MacVicar and Hochman, 1991; Holthoff and Witte, 1996) may also be involved in intrinsic signals at wavelengths >700 nm, at which the absorption coefficients of both HbO_2 and Hbr are relatively small (Maheswari *et al.*, 2003).

Since hemodynamic responses are the basis of modern functional brain imaging techniques such as positron emission tomography (PET) and functional magnetic resonance imaging (fMRI), it is very important to characterize their spatial and temporal properties. Analyses of intrinsic signals at visible wavelengths provide clues that can lead to an understanding of these properties. Malonek and Grinvald (1996) applied spectroscopy to the analysis of intrinsic signals in the cat visual cortex, and found that increases in Hbr concentration were confined to iso-orientation domains, but increases in HbO_2 concentrations were less localized. These results suggest that blood inflow to an activated area is not strongly confined to submillimeter-scale functional domains. However, Duong *et al.* (2001) have recently demonstrated using cerebral-blood-flow (CBF)-based fMRI that blood flow changes are strongly localized to iso-orientation domains in the cat visual cortex. Similarly, an earlier work suggested that blood volume changes associated with changes in blood inflow are localized in active domains (Frostig *et al.* 1990). Thus, the spatial specificities of blood flow changes and associated blood volume changes are still unresolved. In particular, because of the lack of detailed examinations, the specificity of blood volume changes remains unconfirmed. Here, we characterized spatial and temporal patterns of blood volume changes in the cat visual cortex using two methods: (i) intrinsic signal imaging at the wavelength of hemoglobin's isosbestic point, and (ii) imaging of absorption changes of an intravenously injected absorption dye.

Materials and Methods

Eighteen cats (2–6 months of age, 1.0–3.3 kg) were used under anesthesia; five of the animals were also used in the awake state. All procedures were conducted following the 'Guiding Principles for the Care and Use of Animals in the Field of Physiological Sciences' (The